

Discovery of Potent Peptidomimetic Antagonists for Heterochromatin Protein 1 Family Proteins

Kelsey N. Lamb, Sarah N. Dishman, Jarod M. Waybright, Isabelle A. Engelberg, Justin M. Rectenwald, Jacqueline L. Norris-Drouin, Stephanie H. Cholensky, Kenneth H. Pearce, Lindsey I. James, and Stephen V. Frye*



Cite This: *ACS Omega* 2022, 7, 716–732



Read Online

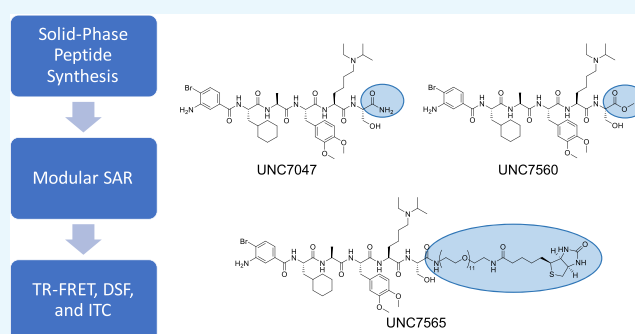
ACCESS |

Metrics & More

Article Recommendations

Supporting Information

ABSTRACT: The heterochromatin protein 1 (HP1) sub-family of CBX chromodomains are responsible for the recognition of histone H3 lysine 9 tri-methyl (H3K9me₃)-marked nucleosomal substrates through binding of the N-terminal chromodomain. These HP1 proteins, namely, CBX1 (HP1 β), CBX3 (HP1 γ), and CBX5 (HP1 α), are commonly associated with regions of pericentric heterochromatin, but recent literature studies suggest that regulation by these proteins is likely more dynamic and includes other loci. Importantly, there are no chemical tools toward HP1 chromodomains to spatiotemporally explore the effects of HP1-mediated processes, underscoring the need for novel HP1 chemical probes. Here, we report the discovery of HP1 targeting peptidomimetic compounds, UNC7047 and UNC7560, and a biotinylated derivative tool compound, UNC7565. These compounds represent an important milestone, as they possess nanomolar affinity for the CBX5 chromodomain by isothermal titration calorimetry (ITC) and bind HP1-containing complexes in cell lysates. These chemical tools provide a starting point for further optimization and the study of CBX5-mediated processes.



INTRODUCTION

The dynamic regulation of chromatin is achieved by several discrete pathways acting in concert with one another: DNA methylation, integration of histone variants, repositioning of nucleosomes through nucleosomal remodeling complexes, recruitment of transcription factors, and histone post-translational modifications (PTMs) all play integral roles in preserving the chromatin landscape.¹ The myriad of chemical modifications elucidated as histone PTMs offer a multifaceted mechanism for chromatin regulation mediated by classes of proteins responsible for their maintenance. One well-studied histone PTM is the methylation of the ϵ -amino group of lysine, commonly referred to as methyl-lysine (Kme). This mark can occur in three different forms: mono- (Kme₁), di- (Kme₂), and trimethyl-lysine (Kme₃), all of which maintain the positive charge of the ϵ -amino group. Depending upon the location and extent of methylation (mono-, di-, or tri-), Kme marks can be associated with both active and repressed chromatin states.^{2,3} Reader proteins that bind this mark are therefore crucial signaling hubs, as they often contribute to and recruit multi-subunit complexes that further modulate the chromatin structure and gene transcription.^{1,4–7}

Several families of reader domains that bind specific Kme residues have been identified and characterized.^{7,8} Among these, chromodomains have emerged as crucial regulators of

histone H3 lysine 9 trimethyl (H3K9me₃) and histone H3 lysine 27 trimethyl (H3K27me₃).⁹ Structural diversity within the chromodomain family has resulted in specificity for one mark versus the other, as the Polycomb (Pc) sub-family of chromobox (CBX) proteins has been shown to primarily bind H3K27me₃, while the heterochromatin protein 1 (HP1) family of CBX chromodomains and MPP8 chromodomain have shown specificity for H3K9me₃. While the function of MPP8 has only recently been appreciated,¹⁰ the recognition of H3K9me₃ and H3K27me₃ by CBX chromodomains has been an active area of study among several groups, including ours.^{9,11–19}

While we and others^{18–25} have made progress toward high-quality chemical probes for the Polycomb CBX proteins, ligands for the HP1 family are lacking and a dedicated effort to create tools to explore the biology of HP1 chromodomains is warranted. The HP1 family includes HP1 α (also known as CBX5), HP1 β (CBX1), and HP1 γ (CBX3), which contain a

Received: September 28, 2021

Accepted: December 7, 2021

Published: December 22, 2021



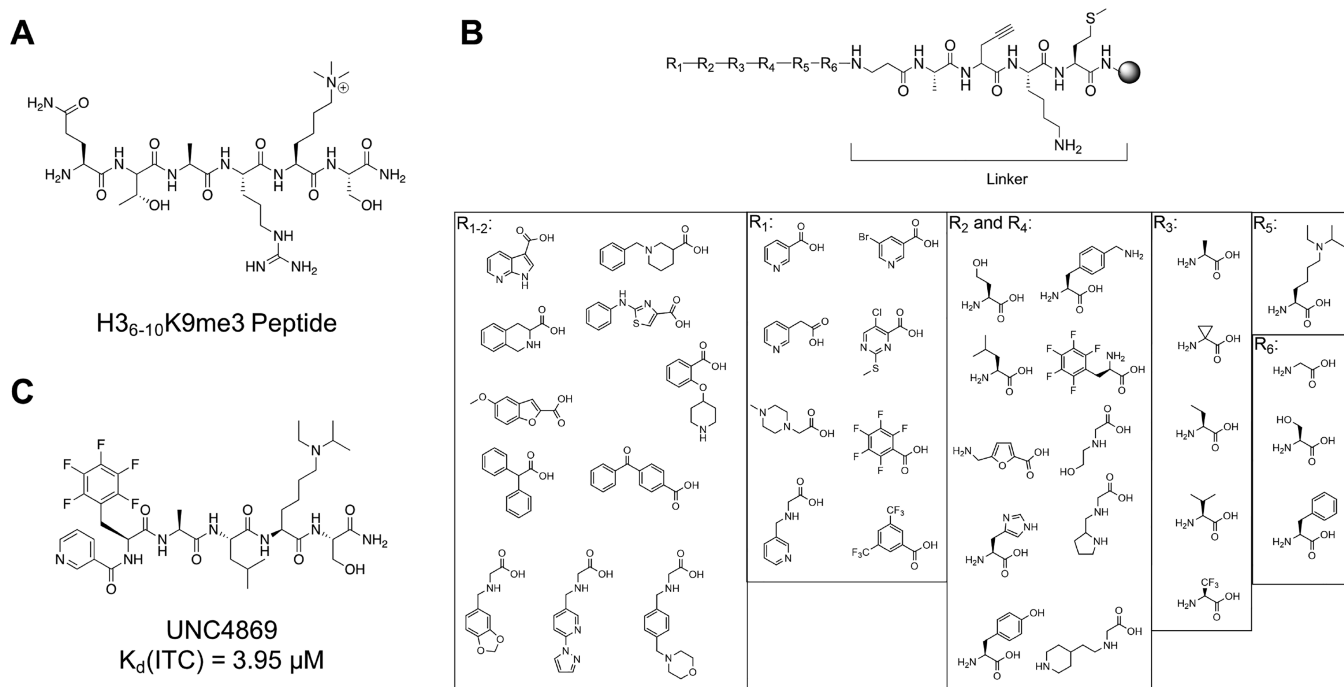


Figure 1. OBOC library assembly for CBX5. (a) Structure of the H36-10K9me3 peptide. (b) CBX5 library design with the general schematic for the library assembly listed above. (c) Structure of UNC4869, a low-micromolar affinity ligand for CBX5 used as a soluble competitor in on-bead screening.

structurally conserved, N-terminal chromodomain consisting of a three-stranded anti-parallel β -sheet motif packed against a C-terminal α -helix. This allows for contacts with the H3K9me3 residue itself as well as the surrounding histone peptide substrate.^{7,13,14,26–28} In addition to the N-terminal chromodomain, HP1 proteins also contain a middle “hinge region” and a unique C-terminal chromoshadow domain that are crucial for HP1-mediated biology.^{29–36} The hinge region, which is rich in basic residues, is known to bind DNA in a non-sequence specific fashion.^{17,35} This allows for multivalent interactions through both H3K9me3 binding to the chromodomain and DNA binding in the hinge region.

The C-terminal chromoshadow domain of the HP1 family is required for homo- and heterodimerization with other HP1 chromoshadow domains, leading to the compaction of nucleosomes and condensation of chromatin.^{37–39} Importantly, the chromoshadow domain reduces non-specific binding to DNA by the hinge region, shifting HP1 occupancy away from unmethylated H3K9 nucleosomes.³⁵ Chromoshadow domain dimerization also enhances HP1 multivalency as it allows multiple chromodomains to interact with adjacent H3K9me3-marked nucleosomes, promoting HP1 enrichment at sites of increased H3K9me3 and subsequently enhancing residence time on chromatin.³⁸ Additionally, the chromoshadow domain dimer structure creates a unique interface through which other HP1 interaction partners can be recruited.^{32,34–36,40} Selection of various peptide binding partners dictates additional downstream functions of HP1-mediated chromatin regulation.^{34,35,40–42}

HP1 proteins have classically been implicated in the formation of pericentric heterochromatin by bridging dinucleosomes through chromoshadow domain dimerization, which leads to the compaction of chromatin.^{43,44} Although this activity is initiated at sites of H3K9me3, HP1 proteins interact with the H3K9 methyltransferases SUV39H1, SUV39H2, and

SETDB1, suggesting the potential for self-propagation of H3K9me3 marks.⁴⁵ Recent literature studies also suggest that HP1 proteins have several H3K9me3-mediated functions outside of pericentric heterochromatin formation. Regulation of gene expression,^{31,46} DNA replication and repair,^{29,47} cell cycle progression,^{32,48,49} cell differentiation, and development have all been implicated as HP1 functions, likely due at least in part to the unique interaction partners that bind at the chromoshadow domain dimer interface.^{32,33,50} While there is relatively limited evidence of HP1 protein misregulation in cancers and other diseases,^{51,52} their essential role for proper chromatin organization during mitosis emphasizes their critical biological function.^{32,48,49}

Despite recent insight into the functions of HP1 proteins, there remains an incomplete understanding of individual and overlapping HP1 homologue activities. Furthermore, to the best of our knowledge there are currently no chemical tools that potently bind any of the HP1 proteins. In comparison to traditional genetic approaches that ablate protein levels and compromise the integrity of multi-subunit protein complexes, chemical probes offer domain-specific insights into the protein function in a spatiotemporally defined fashion.^{53–55} Moreover, this domain-specific perturbation can also inform an individual subunit’s activity within a protein complex without affecting complex stability. We reasoned that antagonizing the binding of the HP1 CBX chromodomains to H3K9me3 could disrupt localization of the protein to its desired target sites and better elucidate the role of HP1 proteins in their multitude of downstream functions.

Here, we describe our efforts toward the development of novel ligands toward the HP1 family chromodomains. Based on the high homology within the HP1 family, we did not anticipate achieving selectivity between the members and focused on CBX5 as a representative target. We first employed a combinatorial chemistry-mediated approach,⁵⁶ utilizing a

previously solved co-crystal structure of the CBX5 chromodomain and an H3K9me3 peptide (PDB: 3FDT) to inspire the library design. Based on the results of this combinatorial library, we screened hit compounds and related analogs by time-resolved fluorescence resonance energy transfer (TR-FRET) and differential scanning fluorimetry (DSF) assays for CBX5 and related chromodomains. Analysis of structure–activity relationships (SAR) allowed us to iteratively optimize potency and selectivity and arrive at peptidomimetic compounds UNC7047 and UNC7560 and a biotinylated derivative tool compound, UNC7565. Importantly, these compounds possess nanomolar affinity for the CBX5 chromodomain and show HP1-specific function in cell lysates.

RESULTS AND DISCUSSION

One-Bead-One-Compound Library Synthesis and Screening for CBX5. To initiate ligand development, we utilized the CBX5 chromodomain crystal structure with the N-terminus of the histone H3K9me3 peptide (PDB: 3FDT) to design a CBX5-directed, one-bead-one-compound (OBOC) combinatorial library. Since our prior ligand development efforts for chromodomains focused on six-residue peptide sequences,^{23–25,56} we narrowed in on the Q6-S10 region of the H3K9me3 (H3₆₋₁₀K9me3) peptide for optimization (Figure 1a). We prioritized both chemical and structural diversity in building the OBOC library to determine whether CBX5 adhered to the same principles for ligand binding as other closely related chromodomains. This was explored in two ways; first, both peptide and peptoid residues were incorporated into the library at certain positions to define CBX5's dependency on interactions with the ligand's amide backbone and to see if the peptidomimetic nature could be attenuated to improve physicochemical properties and enhance cell permeability.^{57,58} Second, we generated a “sub-library” that incorporated fused or bicyclic residues at the N-terminus (R₁₋₂) in another effort to reduce the peptidomimetic nature (Figure 1b).

Starting at the C-terminus at serine 10, we chose to include serine as well as glycine and phenylalanine residues at “R6” to test the necessity for polar contacts between the serine 10 hydroxyl group and the CBX5 carboxyl and amide groups of Glu52 and Asn56, respectively. To reduce the overall complexity of the library, we opted to only include one methyl-lysine mimetic residue, N6-ethyl, N6-isopropyl lysine, at the K9me3 “R5” position, as a previous work in our group demonstrated that this methyl-lysine mimetic both improves affinity and optimizes physicochemical properties by removing the quaternary charge on the lysine amine.⁵⁶ At both the arginine 8 (“R4”) and threonine 6 (“R2”) positions, we incorporated mostly polar and charged peptide and peptoid residues. This was based on the fact that HP1 proteins possess “polar fingers” (Glu19 and Asp58 for CBX5⁹) that clasp over this region of the peptide sequence, creating the possibility for polar or charged contacts with either of these residues in an orientation that improves ligand affinity. The “R3” alanine 7 position is largely conserved in peptide sequences and peptidomimetics bound by chromodomains, as both H3K9me3 and H3K27me3 peptides have an alanine residue situated at this position in relation to trimethyl-lysine. This alanine residue binds in a small “alanine pocket” in many chromodomains,^{9,23} limiting the scope of residues that can realistically be included at this position. Nevertheless, we wanted to explore the tolerance of this alanine pocket in CBX5

for residues smaller and larger than alanine, potentially as a strategy to develop CBX5 selective ligands.^{20,22} Finally, we focused on the N-terminal residue (R1) corresponding to glutamine 6 of the H3₆₋₁₀K9me3 peptide.^{23–25,56} This “capping residue” has proven to be crucial in determining ligand potency and selectivity for other chromodomains, and while not much is known about CBX5's preference in this region, previous CBX5 screening efforts^{56,59} suggested affinity for small heterocyclic aromatic moieties. We elected to incorporate both peptide and peptoid residues at this N-terminal position. As noted previously, to further increase structural diversity, we generated a sub-library containing fused or bicyclic peptide and peptoid residues in place of both residues “R1” and “R2” (denoted by “R₁₋₂”). Following incorporation of “R3”, the compounds in this sub-library were capped with residues from the “R₁₋₂” category.

The CBX5 targeted library was synthesized using split-and-pool synthesis to yield a one-bead-one-compound (OBOC) library format. A linker was installed prior to the incorporation of the library residues (Figure 1b). Placement of methionine as the first residue of the linker enabled CNBr cleavage from the resin for hit deconvolution by MALDI-TOF/TOF MS/MS, while lysine was used to maintain an overall positive charge on bead to prevent aggregation.⁵⁶ The six-residue “traditional” library and five-residue “fused cap” library contained 12,000 and 1650 unique compounds, respectively. The libraries were prepared with approximately 20 copies of each individual compound as we aimed to utilize the recurrence of hit compounds following on-bead screening as a criterion to prioritize compounds for resynthesis. Amino acids were coupled by standard Fmoc solid phase synthesis, while peptoid residues were synthesized by bromoacetic acid coupling and subsequent substitution with a primary amine. Deprotection of the pooled library to remove Boc/tBu groups was conducted under acidic conditions, and the final library was equilibrated in aqueous buffer prior to screening.

Screening was conducted on-bead via magnetic enrichment.^{56,59} CBX5 was first validated in the assay utilizing a positive control compound discovered from a previous combinatorial library, UNC4869 (Figure 1c).⁶⁰ UNC4869 was synthesized on-bead with the standard linker (Figure 1b), and subsequent binding of UNC4869-containing beads to His-tagged CBX5 was completed via the use of an anti-6x-His antibody immobilized on Protein G Dynabeads. After validation of the assay for CBX5, the two sub-libraries were carried through a stringent screening cascade as outlined in Figure S1. The CBX5 chromodomain was screened first, and it was quickly evident that the fused R₁₋₂ cap sub-library did not contain any compounds with high enough affinity to bind the CBX5 chromodomain, suggesting that extended intermolecular hydrogen bonding between the amide backbones of both the protein and peptide are required for maintaining potency.^{23–25,56} Beads that were magnetically enriched in the six-residue library were then treated with a soluble competitor compound, UNC4869 (Figure 1c, off-bead), to elute off low-affinity compounds and retain hits that were equipotent or more potent than UNC4869. Beads competed off by UNC4869 after 1 h were removed while retained hits were cross-screened against CBX7 and MPP8 chromodomains, sequentially. Following the MPP8 cross-screen, beads that were not magnetically enriched in the presence of either protein (“<3hr, (-) CBX7, (-) MPP8” and “>3hr, (-) CBX7, (-) MPP8” in Figure S1) were stripped of protein and subjected to

CNBr-mediated cleavage from the bead for subsequent analysis by MALDI-TOF/TOF tandem mass spectrometry.

Deconvolution of hit sequences by MALDI-TOF/TOF encouragingly revealed multiple redundant compound sequences, suggesting these as true hits for CBX5. Within this set of redundant compounds, structural similarities were visibly present. Notably, no peptoid residues were incorporated into any hit compound identified by MALDI-TOF/TOF, further supporting that backbone H-bonds are critical for affinity.

Two compounds, which were the most highly redundant hit compounds from the screen, were resynthesized on Rink amide resin without the constant linker, cleaved as the C-terminal amide, and subsequently tested by ITC to determine whether they were true hits for CBX5. Satisfyingly, both UNC5154 and UNC5156 displayed low micromolar affinity for CBX5 with K_d values of 4.95 and 3.91 μM , respectively (Figure 2 and Figure S2); however, no apparent affinity gains

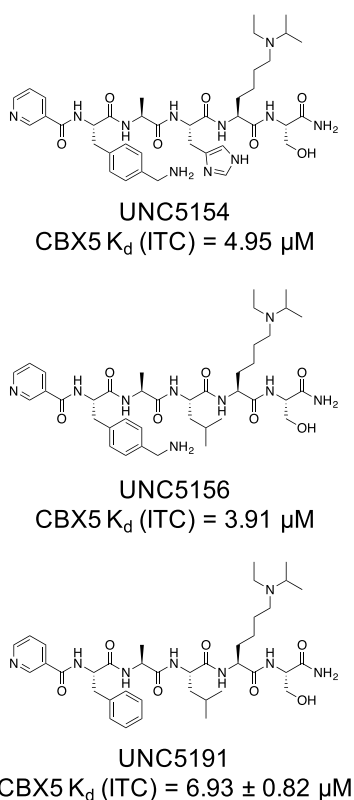


Figure 2. OBOC library resynthesized hits and similar analog, UNC5191. Chemical structures and ITC affinities for closely related analogs, UNC5154 (top), UNC5156 (middle), and UNC5191 (bottom). Data is presented as one individual replicate for UNC5154 and UNC5156 and mean \pm SD of two individual replicates for UNC5191.

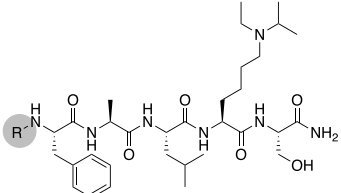
had been made over the soluble competitor control compound, UNC4869. It is possible that higher affinity compounds were filtered out in the CBX7 and MPP8 cross-screening steps as selectivity was a clear priority of our screening efforts.

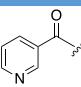
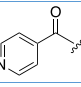
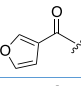
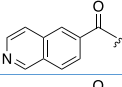
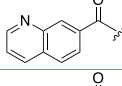
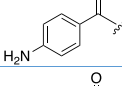
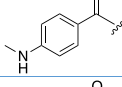
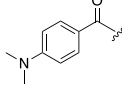
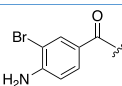
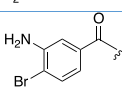
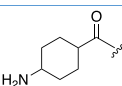
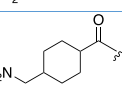
Synthesis and Screening of New Peptidomimetic Ligands for CBX5 Chromodomain. We continued our efforts toward the development of potent CBX5 ligands by pursuing the synthesis of individual peptidomimetic compounds and screening methods that would allow for better quantification of affinity gains. We first wanted to settle on a core scaffold to further explore CBX5 SAR. In analyzing the

affinities of UNC5154 and UNC5156 for CBX5, the leucine at the R4 position of UNC5156 highlighted that polar residues are non-essential at positions of the peptide that contact the polar fingers of CBX5. The hydrophobic leucine also provides more optimal physicochemical properties in comparison to the positively charged histidine of UNC5154, which is more likely to reduce cell permeability.^{57,58} Similarly, we wanted to determine if the aminomethyl portion of 4-aminomethyl phenylalanine was also required for binding. We therefore synthesized UNC5191, which contains a phenylalanine in place of the 4-aminomethyl phenylalanine of UNC5156 (Figure 2 and Figure S2). ITC revealed that the 4-aminomethyl phenylalanine did not make any critical polar contacts, as UNC5191 was only two-fold weaker than UNC5156 (Figure 2 and Figure S2). Importantly, UNC5191 also provided a cost-effective and simple scaffold from which to generate single-point analogues.

Utilizing UNC5191 and SAR from our OBOC approach as a starting point, a series of 22 analogues were synthesized by standard solid phase peptide synthesis (SPPS) techniques, as described previously.⁵⁶ In order to assess newly synthesized analogues of UNC5191, two orthogonal methods were employed to interrogate affinity as well as selectivity. The first method, DSF, allows for the detection of ligand-mediated protein stabilization in response to heat challenge through a fluorescent readout.⁶¹ A CBX5 DSF assay was optimized for screening UNC5191 analogues and the facile interpretation of single amino acid modifications. The second screening method that we chose to employ was a suite of TR-FRET assays already developed for CBX5 and a number of other chromodomains.⁶² While DSF allows for assessment of relative affinity differences via changes in ΔT_m , this assay does not report quantitative affinity values or exploit competition with a tracer unlike TR-FRET. We chose to screen all new compounds via TR-FRET with CBX5, CBX7, and MPP8 chromodomains to mirror our OBOC library screening approach.¹⁰ However, optimized ligands were evaluated in a broader chromodomain panel including the remaining Polycomb chromodomains (CBX2, -4, -6, and -8) and CDYL2.

First, examining the R1 position (Table 1), we wanted to test CBX5's tolerance for other small heterocyclic aromatic cap residues and thus synthesized the 4-pyridyl (UNC6867) and 3-furyl (UNC6389) containing compounds. Both modifications were tolerated according to CBX5 TR-FRET and DSF assays. We then expanded this ring structure to test nitrogen-containing bicyclic caps including isoquinoline (UNC6391) and quinoline (UNC6390). These analogues were also tolerated and demonstrated a 4- to 5-fold improved affinity over UNC5191. Unfortunately, none of these four compounds displayed improved selectivity for CBX5 over CBX7 and MPP8. We then moved the amine outside of the ring to generate 4-amino- (UNC6393), 4-(methylamino)- (UNC6394), and 4-(dimethylamino)-benzyl (UNC6386) caps while also examining the effects of an additional halogen on the ring with 4-amino-3-bromobenzyl (UNC6387) and 3-amino-4-bromobenzyl (UNC6868) caps. While all of these modifications were well tolerated, overall, none of these compounds exhibited enhanced selectivity for CBX5 over both CBX7 and MPP8. Encouragingly, UNC6868 was the first compound tested against CBX5 to display nanomolar affinity by TR-FRET and presented the highest ΔT_m shift (~ 9 $^{\circ}\text{C}$). To round out exploration at the cap residue, UNC6393 was

Table 1. DSF and TR-FRET Data for R₁ Position^a


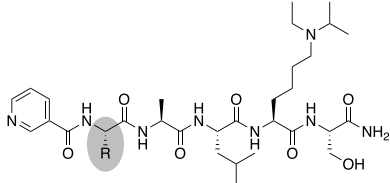
UNC ID	R	CBX5 DSF ΔTm (°C)	CBX5 IC ₅₀ (μM)	CBX7 IC ₅₀ (μM)	MPP8 IC ₅₀ (μM)
UNC5191		1.8 ± 0.13	6.4 ± 1.5	25 ± 13	2.2 ± 0.54
UNC6867		3.0 ± 0.42	5.7 ± 1.8	9.4 ± 3.5	0.99 ± 0.09
UNC6389		2.7 ± 0.65	4.3 ± 0.69	6.8 ± 1.9	1.2 ± 0.23
UNC6390		5.3 ± 0.98	1.1 ± 0.04	1.5 ± 0.30	0.42 ± 0.08
UNC6391		5.3 ± 1.0	1.4 ± 0.46	3.5 ± 1.2	0.64 ± 0.07
UNC6393		4.6 ± 0.79	3.1 ± 0.33	3.8 ± 0.73	1.8 ± 0.12
UNC6394		5.6 ± 0.54	4.6 ± 0.68	2.8 ± 0.65	4.4 ± 0.63
UNC6386		4.9 ± 0.46	1.4 ± 0.57	0.20 ± 0.11	0.38 ± 0.16
UNC6387		5.0 ± 0.76	1.4 ± 0.31	3.2 ± 2.2	0.40 ± 0.07
UNC6868		8.9 ± 0.23	0.63 ± 0.12	0.21 ± 0.05	0.29 ± 0.07
UNC6865		0.53 ± 0.11	52 ± 8.4	35 ± 13	0.42 ± 0.11
UNC6866		0.55 ± 0.27	93 ± 13	20 ± 6.9	1.8 ± 0.37

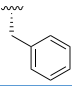
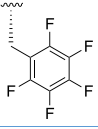
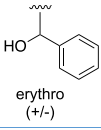
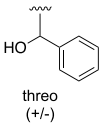
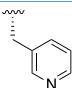
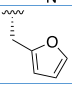
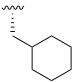
^aThe residue of UNC5191 being modified is highlighted with a gray circle above the data table. Both DSF and TR-FRET data is presented as mean ± SD of three individual assay replicates.

de-aromatized in UNC6865 and the amine was further extended outside of the de-aromatized ring with the 4-(aminomethyl)cyclohexyl cap (UNC6866). Loss of aromaticity caused almost complete ablation of CBX5 binding (Table 1), emphasizing a requirement for aromaticity at the cap position.

We then shifted our focus to the R2 position of UNC5191, which harbors a phenylalanine residue while maintaining the 3-pyridyl capping residue (Table 2). We chose to incorporate largely aromatic residues at this position. UNC4869, our soluble competitor from OBOC library screening, is a close analog of UNC5191 with a pentafluorophenylalanine residue at the R2 position. UNC4869 binds CBX5 about 3-fold more

potently by TR-FRET and also demonstrates a boost in selectivity over CBX7, suggesting a preference for electron-deficient aromatics at this position. Incorporation of erythro-(UNC6377) and threo-β-phenylserine (UNC6378) were explored to test whether polar contacts could be formed between these residues and the polar fingers⁹ of CBX5. There is a clear conformational preference for the threo-β-phenylserine residue, which likely maintains the extended β-sheet structure of the peptidomimetic sequence; however, no significant affinity gains due to added polarity were observed. 3-(3-Pyridyl)-alanine (UNC6381) and 3-(2-furyl)-alanine (UNC6382) were examined to look at the tolerance of heterocyclic aromatic residues at this position. While

Table 2. DSF and TR-FRET Data for R₂ Position^a


UNC ID	R	CBX5 DSF ΔT_m (°C)	CBX5 IC ₅₀ (μ M)	CBX7 IC ₅₀ (μ M)	MPP8 IC ₅₀ (μ M)
UNC5191		1.8 ± 0.13	6.4 ± 1.5	25 ± 13	2.2 ± 0.54
UNC4869		4.7 ± 0.31	2.4 ± 0.54	62 ± 22	1.6 ± 0.44
UNC6377	 erythro (+/-)	-0.74 ± 0.20	> 100	> 100	76 ± 6.9
UNC6378	 threo (+/-)	1.8 ± 0.33	3.9 ± 0.68	9.3 ± 2.1	1.9 ± 0.27
UNC6381		2.5 ± 0.53	4.1 ± 0.80	52 ± 36	1.8 ± 0.24
UNC6382		1.2 ± 0.33	42 ± 14	46 ± 12	11 ± 0.68
UNC6383		2.8 ± 0.51	2.5 ± 0.37	28 ± 8.6	1.5 ± 0.27

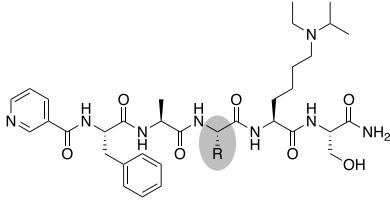
^aThe residue of UNC5191 being modified is highlighted with a gray circle above the data table. Both DSF and TR-FRET data is presented as mean \pm SD of three individual assay replicates.

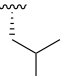
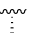
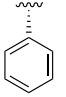
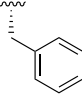
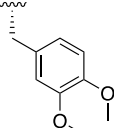
UNC6381 maintained activity for CBX5, it is likely that the 3-(2-furyl)-alanine residue of UNC6382 is disrupting the hydrogen bonding network between the compound's peptide backbone and the backbone of CBX5, thus attenuating affinity. We also tested CBX5's dependency on aromaticity at the R2 residue by incorporation of cyclohexylalanine (UNC6383). The slight increase in affinity suggests that aromaticity is not required so long as lipophilicity is maintained. UNC4869 and UNC6383 demonstrated the highest selectivity for CBX5 over CBX7, with 26-fold and 11-fold selectivities, respectively. Unfortunately, selectivity over MPP8 remained elusive. It is also worth noting that UNC4869 solubility was poor, presumably due to the bulky, lipophilic, pentafluorophenylalanine group.

Finally, we focused on modifications to the R4 position of UNC5191 (Table 3). Since there is a leucine at this position in UNC5191, we chose to explore primarily lipophilic residues with increasing size. We therefore synthesized compounds incorporating alanine (UNC6379), 2-phenylglycine (UNC6380), phenylalanine (UNC6384), and 3,4-dimethoxyphenylalanine (UNC6392). With the exception of UNC6380, it was evident from both TR-FRET and DSF data that increasing the size at this position yielded corresponding

increases in affinity for CBX5. Unfortunately, this trend persisted for CBX7 and MPP8 as well, thus limiting gains in CBX5 selectivity. It is worth noting that while TR-FRET suggested that UNC6384 and UNC6392 are equipotent for CBX5, DSF registered a ~ 3 °C ΔT_m difference between the two compounds (Table 3) suggesting a higher affinity for UNC6392. This was subsequently investigated by ITC, revealing that UNC6392 ($K_d = 1.27 \mu\text{M}$) is 2-fold more potent than UNC6384 ($K_d = 3.38 \mu\text{M}$, Figure S3). The data from this set of analogs modified at the R4 position of UNC5191 demonstrates the importance of utilizing multiple in vitro screening methods when possible for efficient rank ordering of newly synthesized compounds.

Given the encouraging results from manipulating individual residues in the UNC5191 scaffold, we next synthesized a compound that combined the most advantageous alterations at each position. This yielded UNC7047, which harbors a 3-amino-4-bromobenzyl cap in place of the 3-pyridyl cap at the R1 position, a cyclohexylalanine in place of phenylalanine at R2, and 3,4-dimethoxyphenylalanine in place of leucine at R4. The 3-amino-4-bromobenzyl cap was selected primarily due to the 10-fold increase in affinity over UNC5191, as selectivity was unattainable at this position. Meanwhile, the cyclo-

Table 3. DSF and TR-FRET Data for R₄ Position^a


UNC ID	R	CBX5 DSF ΔT_m ($^{\circ}\text{C}$)	CBX5 IC ₅₀ (μM)	CBX7 IC ₅₀ (μM)	MPP8 IC ₅₀ (μM)
UNC5191		1.8 ± 0.13	6.4 ± 1.5	25 ± 13	2.2 ± 0.54
UNC6379		1.9 ± 0.23	11 ± 2.4	98 ± 3.7	3.4 ± 0.52
UNC6380		1.1 ± 0.35	16 ± 3.2	36 ± 25	2.2 ± 0.63
UNC6384		4.3 ± 0.41	1.5 ± 0.32	27 ± 18	0.55 ± 0.13
UNC6392		7.1 ± 0.77	1.3 ± 0.21	8.2 ± 1.6	1.9 ± 0.19

^aThe residue of UNC5191 being modified is highlighted with a gray circle above the data table. Both DSF and TR-FRET data is presented as mean ± SD of three individual assay replicates.

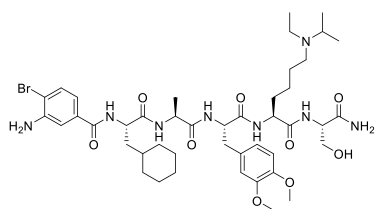
hexylalanine and 3,4-dimethoxyphenylalanine were selected due to a combination of affinity and selectivity gains and better physicochemical space. By TR-FRET, this compound displayed an 80-fold affinity enhancement toward CBX5 in comparison to UNC5191, and DSF showed an increase in the T_m of CBX5 by more than 14 $^{\circ}\text{C}$, which is 12 $^{\circ}\text{C}$ more than the shift observed with our starting ligand, UNC5191 (Figure 3). Although the K_d of UNC7047 for CBX5 was slightly diminished versus its IC₅₀ (ITC K_d = 237 ± 68 nM, Figure 3 and Figure S4, TR-FRET IC₅₀ (79 ± 40 nM)), UNC7047 is

still 30-fold more potent than UNC5191 (ITC K_d = 6.93 ± 0.82 μM , Figure 2 and Tables 1–3), which was achieved in just one round of modular SAR.

Owing to previous data from our group suggesting that C-terminal methyl ester derivatives of peptidomimetic compounds are more efficacious in cellular contexts than the corresponding amides,^{18,23,24} we synthesized our top hit compound, UNC7047, as a methyl ester (UNC7560, Table 4) for further analysis. Gratifyingly, UNC7560 maintains near identical potency toward CBX5 in comparison to the C-terminal amide compound, UNC7047, by both TR-FRET and ITC (Figure 3, Table 4, and Figure S5).

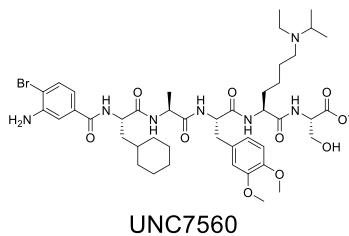
To more stringently examine the selectivity of UNC7560, we evaluated UNC7560 binding to several other chromodomains *in vitro* via a combination of both TR-FRET and ITC assays. Our original TR-FRET panel of CBX5, CBX7, and MPP8 chromodomains was expanded to include additional Polycomb chromodomains including CBX2, CBX4, CBX6, and CBX8, as well as the closely related chromodomain, CDYL2. As we did not have CBX1 and CBX3 TR-FRET assays available in house, we utilized ITC to profile these two chromodomains, as well as CBX5, CBX7, MPP8, and CDYL2. ITC revealed that UNC7560 binds the other HP1 family members, CBX1 and CBX3, nearly as potently as CBX5 (Table 4 and Figure S5). This was expected based on sequence homology among the HP1 family chromodomains, which likely presents a high barrier toward HP1 isoform-specific chemical probes.³⁰

UNC7560 binding data for the Polycomb CBXs (CBX2, -4, -6, -7, and -8) revealed a similar trend to that seen with



UNC7047
CBX5 DSF ΔT_m ($^{\circ}\text{C}$) = 14.5 ± 0.55
CBX5 TR-FRET IC ₅₀ (μM) = 0.079 ± 0.04
CBX7 TR-FRET IC ₅₀ (μM) = 0.18 ± 0.02
MPP8 TR-FRET IC ₅₀ (μM) = 0.20 ± 0.004
CBX5 ITC K_d (μM) = 0.24 ± 0.068

Figure 3. UNC7047 structure and *in vitro* assay data. DSF, TR-FRET, and ITC data for the optimized compound, UNC7047. Data is presented as mean ± SD of three individual replicates for each DSF, TR-FRET, and ITC assay.

Table 4. TR-FRET and ITC Data for UNC7560 Selectivity Profiling^a


UNC7560

Chromodomain	TR-FRET IC ₅₀ (μM)	ITC K _d (μM)	
HP1 Family	CBX5 (HP1α)	0.13 ± 0.013	0.28 ± 0.025 (n=2)
	CBX1 (HP1β)		0.48 ± 0.00 (n=2)
	CBX3 (HP1γ)		0.42 ± 0.040 (n=2)
Polycomb Family	CBX2	2.00 ± 0.19	
	CBX4	0.28 ± 0.032	
	CBX6	0.81 ± 0.028	
	CBX7	0.34 ± 0.030	2.06 ± 1.39 (n=2)
	CBX8	0.89 ± 0.16	
Other Chromodomains	MPP8	0.50 ± 0.035	23* (n=1)
	CDYL2	0.028 ± 0.0035	0.96 ± 0.34 (n=2)

^aTR-FRET data is presented as mean ± SD of three individual assay replicates. ITC data is presented as mean ± SD of at least two individual assay replicates.

previous CBX7-targeted chemical probes from our group, UNC3866 and UNC4976.^{23,25} UNC7560 is equipotent toward CBX4 and CBX7 and exhibits a three-fold drop in potency toward CBX6 and CBX8 and a six-fold drop toward CBX2 (Table 4 and Figure S6). This is anticipated given that CBX4 and CBX7 prefer lipophilicity at the para-position of the N-terminal cap, which is a *t*-butyl group in both UNC3866 and UNC4976 and a bromo-group in UNC7560.^{23,25} While TR-FRET suggests a two-fold decrease in CBX4/7 affinity in comparison to CBX5, ITC shows about a 9-fold difference between CBX5 and CBX7 binding affinities (Table 4, Figures S5 and S6). As ITC is considered the gold standard for determining in vitro affinity between protein and ligand substrates as a direct measure of binding affinity, we rely on these values for selectivity assessment. Previous work from our group suggests CBX7 ITC analysis to be a suitable proxy into the trend among Polycomb proteins.^{23,25}

UNC7560 potency data for the MPP8 and CDYL2 chromodomains by TR-FRET and ITC reveal that while MPP8 shows a sub-micromolar IC₅₀ for UNC7560 in a competition TR-FRET assay (Table 4 and Figure S6), it displayed weak affinity by ITC (K_d of 23 μM in one replicate of ITC, while two other replicates showed no binding to UNC7560 even at high protein concentrations) (Table 4 and Figure S7). Likewise, UNC7560 demonstrates a low-nanomolar affinity by IC₅₀ in TR-FRET versus CDYL2 while its affinity is ~1 μM by ITC. As noted above, the ITC values should be taken as closest to the true binding affinity and uninfluenced by bait ligand affinity (Table 4, Figure S5). Taken altogether, while UNC7560 is only modestly selective by ITC for the HP1 chromodomains over Polycomb CBXs, CDYL2, and MPP8, evaluation of UNC7560 in cellular contexts should provide insight into HP1-mediated biology, especially in established HP1-mediated contexts.

CHEMIPRECIPITATION OF HP1 Proteins and Interaction Partners. Despite the lack of significant selectivity of UNC7560 over a broad panel of chromodomains, the dramatic increase in affinity for CBX5 prompted us to explore this compound in the context of cellular lysates. Our group has previously utilized PEG-biotin derivatives of our chemical probes to enable chemiprecipitation of Kme reader proteins and associated protein complexes, as Kme reader proteins lack enzymatic activity that is more readily attributable in cells.^{23,25,56}

First, we prepared a PEG₁₁-biotin derivative of UNC7047 (UNC7565, Figure 4a). Based on previous work from our

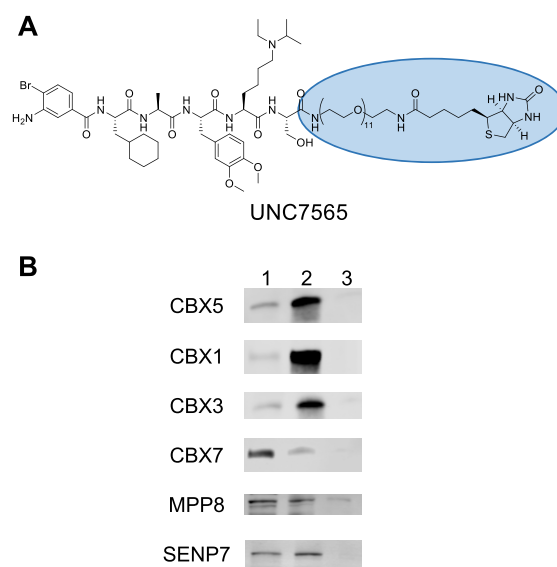


Figure 4. HEK293T lysate pulldown experiments with the UNC7565 biotinylated compound and UNC7560 soluble competitor. (a) Structure of UNC7565. (b) Western blots highlighting bands of interest from HEK293T lysate pulldowns with UNC7565 +/- UNC7560 soluble competitor. 1 = HEK293T lysate input, 2 = UNC7565 pulldown, 3 = UNC7565 pulldown with pre-treatment of UNC7560 soluble competitor. Western blots shown are representative of two replicate experiments.

group, appending a PEG₁₁-biotin tag to the C-terminus of peptidomimetic ligands has negligible effects on chromodomain binding.^{23,25} Utilizing UNC7565, we probed target engagement in cell lysates for all three HP1 CBXs (CBX1 (HP1β), CBX3 (HP1γ), and CBX5 (HP1α)), as well as CBX7 and MPP8 (Figure 4b). Additionally, we also examined the ability of UNC7565 to pulldown a known HP1 interaction partner, the SUMO-protease SENP7,^{33,50} which interacts with HP1 proteins through binding to the chromoshadow domain. Chemiprecipitation from HEK293T cell lysates revealed successful pulldown of all three HP1 proteins, CBX7, and MPP8. It is worth noting that the three HP1 family proteins

were strongly enriched over input upon chemiprecipitation with UNC7565 in contrast to CBX7 and MPP8 (Figure 4b, lane 2), potentially suggesting increased potency and selectivity for HP1 proteins in cellular contexts versus these other chromodomains. Importantly, UNC7565-mediated pull-down of all chromodomains tested was inhibited by pre-treatment of cell lysates with the untagged compound, UNC7560 (Figure 4b, Lane 3), suggesting that chromodomain-specific interactions are responsible for chemiprecipitation. Excitingly, SENP7 was also pulled-down upon treatment with UNC7565, suggesting that our ligands can engage intact HP1 protein complexes.

DISCUSSION

Our efforts toward the development of more potent CBX5 chromodomain ligands resulted in the novel CBX5 antagonist UNC7047 through a combination of two distinct approaches. First, the development and screening of an OBOC combinatorial library yielded low micromolar hits for CBX5, one of which was developed into a scalable, cost-effective scaffold for subsequent SPPS-mediated analog synthesis. Second, we pursued analog synthesis and *in vitro* screening by TR-FRET and DSF assays. Encouragingly, follow up affinity characterization by ITC revealed a 30-fold increase in CBX5 affinity after just one round of analogue synthesis, underscoring the importance of combining individual modifications in the highly modular peptidomimetic scaffold to achieve additive increases in affinity. One caveat to these studies is the limited selectivity of UNC7047, as the compound is nearly equipotent for CBX5, CBX7, and MPP8 by ITC. While addressing this deficit will be an emphasis of a future work, we expect a rather high barrier to achieving CBX5 selectivity due to the level of sequence conservation among chromodomains.

From the C-terminal amide compound, UNC7047, we created methyl ester (UNC7560) and PEG₁₁-biotin (UNC7565) derivatives. The methyl ester derivative mirrored UNC7047 potency against CBX5 by ITC while also revealing that our optimized compound potently binds the other HP1 family members, CBX1 (HP1 β) and CBX3 (HP1 γ). This capacity to bind CBX5 and other HP1 family members was maintained in cell lysates, as UNC7565-mediated chemiprecipitation revealed robust interactions with all three family members. These results were anticipated due to the highly-conserved structure among this protein family. The N-terminal chromodomain and a C-terminal chromoshadow domain of HP1 proteins comprise approximately 60% of the full length protein, and the degrees of conservation among the chromodomain and chromoshadow domains of HP1 isoforms are 70 and 80%, respectively. This high percentage of conservation provides limited opportunity for isoform-specific activity and may account for some redundant roles of these proteins.^{9,30} However, HP1 isoforms still possess unique functions and are thought to be involved in varying degrees of gene repression, supporting a scenario where HP1 proteins likely maintain a delicate balance between isoform-specific responsibilities and functional redundancy. Overall, this encourages further work toward isoform-selective antagonists.

Encouragingly, while UNC7560 showed high *in vitro* affinity for Polycomb CBXs, lower levels of CBX7 chemiprecipitation were seen in comparison to HP1 CBXs. While further development of HP1-specific antagonists that avoid Polycomb affinity are warranted, HP1 and Polycomb proteins have distinct cellular functions that would be expected to differ

biologically.^{29,63,64} Cellular phenotypes suspected to be due to off-target Polycomb activity can also readily be probed by looking at Polycomb-specific target genes.²⁵

The discovery of UNC7047 marks an important milestone in the development of potent CBX5 chromodomain ligands and should encourage further investigation into both selective and cellularly active antagonists for CBX5 and other HP1 isoforms. As the attention on chromatin regulatory proteins and the histone PTMs that they regulate continues to boom, chemical tools will undoubtedly contribute dramatically to the investigation of target biology, validation of therapeutic targets, and identification of chemical matter to facilitate subsequent therapeutic development. Specifically, a high-quality chemical probe for CBX5 and other HP1 chromodomains would undoubtedly have a significant impact on the elucidation of HP1 biology and clarify the therapeutic tractability of this protein family.

EXPERIMENTAL SECTION

Solid Phase Peptide Synthesis (SPPS) of Hits from the OBOC Library and New CBX5 Compounds. Fmoc-protected amino acids were purchased from Chem-Impex and Sigma-Aldrich with the exception of the Fmoc lysine derivatives, which were synthesized as described previously.⁵⁶ All other chemicals and solvents were purchased from TCI America and Sigma Aldrich.

Synthesis was conducted via solid-phase peptide synthesis on Fmoc Rink amide resin (50 mg, Chem-Impex). The resin was initially swollen in DCM followed by DMF (10 min each). Fmoc deprotection was conducted by incubation with a solution of 2.5% 1,8-diazabicycloundec-7-ene and 2.5% pyrrolidine in DMF for 10 min. The resin was filtered and washed twice with DMF, methanol, DMF, and DCM before amino acid for coupling. Standard Fmoc synthesis protocols were used to generate the six residue peptidomimetics. Briefly, Fmoc-protected amino acids (4 equiv) were mixed for 5 min with HBTU (4 equiv), HOAt (4 equiv), and DIPEA (8 equiv) in 1 mL of DMF and 1 mL of dichloromethane (DCM). The solution was then added to the resin and left on a shaker at room temperature for 1 h. The resin was filtered and washed twice with DCM, DMF, methanol, and DMF again. Fmoc amino acid protecting groups were removed as described above, and then the resin was filtered and washed twice with DMF, methanol, DMF, and DCM before adding the next amino acid for coupling. Following installation of the carboxylic acid capping residue, the resin was rinsed 6 times with DCM. Cleavage cocktail (95% trifluoroacetic acid, 2.5% triisopropylsilane, and 2.5% water) was added to the resin; the mixture was left on the shaker for 2 h; and the filtrate was collected. The resin was rinsed twice with DCM, and the filtrates were pooled and concentrated under vacuum.

The crude material was purified by preparative HPLC using an Agilent Prep 1200 series with the UV detector set to 220 and 254 nm. Samples were injected onto a Phenomenex Luna 75 × 30 mm, 5 μ m, C18 column at 25 °C. Mobile phases of A (H₂O + 0.1% TFA) and B (CH₃CN) were used with a flow rate of 30 mL/min. Product fractions were pooled and concentrated to afford title compounds as TFA salts with yields as indicated in each compound characterization.

Analytical LCMS and ¹H NMR were used to establish purity. Analytical LCMS data was acquired using either an Agilent 6110 Series (UNC5191-UNC6868) or an Agilent 6125 Series (UNC4869, UNC7047-UNC7565) system with the UV

detector set to 220 and 254 nm. Samples were injected (3–5 μ L) onto an Agilent Eclipse Plus 4.6 \times 50 mm, 1.8 μ m, C18 column at 25 $^{\circ}$ C. Mobile phases A (H_2O + 0.1% acetic acid) and B (Agilent 6110: CH_3OH + 0.1% acetic acid; Agilent 6125: CH_3CN + 1% H_2O + 0.1% acetic acid) were used with a linear gradient from 10 to 100% B in 5.0 min followed by a flush at 100% B for another 2.0 min at a flow rate of 1.0 mL/min. Mass spectra (MS) data were acquired in positive ion mode using either an Agilent 6110 or an Agilent 6125 (see above) single quadrupole mass spectrometer with an electrospray ionization (ESI) source. Nuclear magnetic resonance (NMR) spectra were recorded on a Varian Mercury spectrometer at 400 MHz for proton (^1H NMR); chemical shifts are reported in ppm (δ) relative to residual protons in deuterated solvent peaks. Due to intramolecular hydrogen-bonding, hydrogen-deuterium exchange between the amide protons of the molecule and the deuterated solvent is slow and requires overnight equilibration for near complete exchange.

N-((8*S*,11*S*,14*S*,17*S*)-8-(((*S*)-1-Amino-3-hydroxy-1-oxopropan-2-yl)carbonyl)-3-ethyl-11-isobutyl-2,14-dimethyl-10,13,16-trioxo-18-(perfluorophenyl)-3,9,12,15-tetraazaocadecan-17-yl)nicotinamide (UNC4869). The above general procedure yielded 25.7 mg of the title compound as a white solid. ^1H NMR (400 MHz, methanol- d_4) δ 9.02 (s, 1H), 8.76 (s, 1H), 8.33 (d, J = 8.0 Hz, 1H), 7.65 (dd, J = 8.0, 5.1 Hz, 1H), 4.84–4.78 (m, 1H), 4.41–4.29 (m, 4H), 3.87–3.64 (m, 3H), 3.40 (dd, J = 13.9, 7.1 Hz, 1H), 3.28–2.96 (m, 5H), 1.98–1.42 (m, 9H), 1.41–1.30 (m, 12H), 0.98–0.90 (m, 6H). MSI (ESI): 829 [$\text{M} + \text{H}$] $^+$, 415 [$\text{M} + 2\text{H}$] $^{2+}$. t_{R} = 3.14 min.

N-((8*S*,11*S*,14*S*,17*S*)-8-(((*S*)-1-Amino-3-hydroxy-1-oxopropan-2-yl)carbonyl)-3-ethyl-11-isobutyl-2,14-dimethyl-10,13,16-trioxo-18-phenyl-3,9,12,15-tetraazaocadecan-17-yl)nicotinamide (UNC5191). The above general procedure yielded 21.9 mg (70.6%) of the title compound as a white solid. ^1H NMR (400 MHz, methanol- d_4) δ 8.97 (d, J = 1.7 Hz, 1H), 8.76 (dd, J = 5.1, 1.5 Hz, 1H), 8.36 (dt, J = 8.0, 1.9 Hz, 1H), 7.72–7.66 (m, 1H), 7.35–7.25 (m, 4H), 7.24–7.18 (m, 1H), 4.84–4.78 (m, 1H), 4.42–4.29 (m, 4H), 3.88–3.74 (m, 2H), 3.71–3.63 (m, 1H), 3.30–2.96 (m, 6H), 1.99–1.44 (m, 9H), 1.39 (d, J = 7.2 Hz, 3H), 1.35–1.28 (m, 9H), 0.98–0.88 (m, 6H). MSI (ESI): 739 [$\text{M} + \text{H}$] $^+$, 370 [$\text{M} + 2\text{H}$] $^{2+}$. t_{R} = 2.61 min.

N-((8*S*,11*S*,14*S*,18*R*)-8-(((*S*)-1-Amino-3-hydroxy-1-oxopropan-2-yl)carbonyl)-3-ethyl-18-hydroxy-11-isobutyl-2,14-dimethyl-10,13,16-trioxo-18-phenyl-3,9,12,15-tetraazaocadecan-17-yl)nicotinamide (UNC6377). The above general procedure yielded 2.1 mg (4.9%) of the title compound as a white solid. ^1H NMR (400 MHz, methanol- d_4) δ 9.05 (d, J = 11.6 Hz, 1H), 8.74 (d, J = 5.0 Hz, 1H), 8.43–8.31 (m, 1H), 7.98 (s, 1H), 7.63 (dd, J = 8.0, 5.0 Hz, 1H), 7.52–7.42 (m, 2H), 7.36–7.25 (m, 2H), 5.58–5.44 (m, 1H), 4.55 (dd, J = 20.8, 4.8 Hz, 1H), 4.41–4.17 (m, 4H), 3.87–3.65 (m, 3H), 3.29–3.01 (m, 4H), 2.02–1.41 (m, 9H), 1.38–1.31 (m, 9H), 1.28 (s, 2H), 1.03 (d, J = 7.1 Hz, 1H), 0.99–0.88 (m, 6H). MSI (ESI): 755 [$\text{M} + \text{H}$] $^+$, 378 [$\text{M} + 2\text{H}$] $^{2+}$. t_{R} = 3.94 min.

N-((8*S*,11*S*,14*S*,18*S*)-8-(((*S*)-1-Amino-3-hydroxy-1-oxopropan-2-yl)carbonyl)-3-ethyl-18-hydroxy-11-isobutyl-2,14-dimethyl-10,13,16-trioxo-18-phenyl-3,9,12,15-tetraazaocadecan-17-yl)nicotinamide (UNC6378). The above general procedure yielded 1.44 mg (3.41%) of the title compound as a white solid. ^1H NMR (400 MHz, methanol- d_4) δ 8.90 (s, 1H), 8.70 (d, J = 5.0 Hz, 1H), 8.18 (dt, J = 8.0, 1.8 Hz, 1H), 7.56 (dd, J = 8.0, 5.0 Hz, 1H), 7.48 (d, J = 7.5 Hz, 2H), 7.33 (t, J =

7.5 Hz, 2H), 7.29–7.22 (m, 1H), 5.38 (d, J = 3.9 Hz, 1H), 4.88 (d, J = 3.6 Hz, 1H), 4.44–4.27 (m, 4H), 3.86–3.73 (m, 2H), 3.72–3.62 (m, 1H), 3.28–2.93 (m, 4H), 2.01–1.44 (m, 9H), 1.41 (d, J = 7.2 Hz, 3H), 1.37–1.30 (m, 9H), 0.98–0.88 (m, 6H). MSI (ESI): 755 [$\text{M} + \text{H}$] $^+$, 378 [$\text{M} + 2\text{H}$] $^{2+}$. t_{R} = 3.82 min.

N-((8*S*,11*S*,14*S*,17*S*)-8-(((*S*)-1-Amino-3-hydroxy-1-oxopropan-2-yl)carbonyl)-3-ethyl-2,11,14-trimethyl-10,13,16-trioxo-18-phenyl-3,9,12,15-tetraazaocadecan-17-yl)nicotinamide (UNC6379). The above general procedure yielded 5.73 mg (14.5%) of the title compound as a white solid. ^1H NMR (400 MHz, methanol- d_4) δ 8.89 (d, J = 1.6 Hz, 1H), 8.68 (dd, J = 4.9, 1.6 Hz, 1H), 8.18 (ddd, J = 8.0, 2.2, 1.7 Hz, 1H), 7.54 (ddd, J = 8.0, 5.0, 0.8 Hz, 1H), 7.35–7.26 (m, 4H), 7.25–7.18 (m, 1H), 4.82–4.76 (m, 1H), 4.41–4.23 (m, 4H), 3.87–3.75 (m, 2H), 3.73–3.61 (m, 1H), 3.30–2.96 (m, 6H), 1.98–1.45 (m, 6H), 1.42 (d, J = 7.2 Hz, 3H), 1.39 (d, J = 7.2 Hz, 3H), 1.36–1.29 (m, 9H). MSI (ESI): 697 [$\text{M} + \text{H}$] $^+$, 349 [$\text{M} + 2\text{H}$] $^{2+}$. t_{R} = 3.24 min.

N-((8*S*,11*S*,14*S*,17*S*)-8-(((*S*)-1-Amino-3-hydroxy-1-oxopropan-2-yl)carbonyl)-3-ethyl-2,14-dimethyl-10,13,16-trioxo-11,18-diphenyl-3,9,12,15-tetraazaocadecan-17-yl)nicotinamide (UNC6380). The above general procedure yielded 4.3 mg (10%) of the title compound as a white solid. ^1H NMR (400 MHz, methanol- d_4) δ 8.82 (d, J = 15.3 Hz, 1H), 8.66 (d, J = 3.3 Hz, 1H), 8.08 (dt, J = 18.0, 8.0, 2.0 Hz, 1H), 7.53–7.16 (m, 11H), 5.37 (d, J = 26.5 Hz, 1H), 4.46–4.30 (m, 4H), 3.90–3.57 (m, 3H), 3.29–2.82 (m, 6H), 2.00–1.25 (m, 18H). MSI (ESI): 759 [$\text{M} + \text{H}$] $^+$, 380 [$\text{M} + 2\text{H}$] $^{2+}$. t_{R} = 3.76 min.

N-((8*S*,11*S*,14*S*,17*S*)-8-(((*S*)-1-Amino-3-hydroxy-1-oxopropan-2-yl)carbonyl)-3-ethyl-11-isobutyl-2,14-dimethyl-10,13,16-trioxo-18-(pyridin-3-yl)-3,9,12,15-tetraazaocadecan-17-yl)nicotinamide (UNC6381). The above general procedure yielded 5.5 mg (13%) of the title compound as a white solid. ^1H NMR (400 MHz, methanol- d_4) δ 8.99 (s, 1H), 8.81 (s, 1H), 8.78–8.69 (m, 2H), 8.52 (d, J = 8.2 Hz, 1H), 8.34 (dt, J = 8.1, 1.8 Hz, 1H), 7.96 (dd, 1H), 7.65 (dd, 1H), 4.98 (dd, J = 8.2, 6.2 Hz, 1H), 4.43–4.28 (m, 4H), 3.87–3.74 (m, 2H), 3.74–3.66 (m, 1H), 3.53 (dd, J = 14.2, 6.1 Hz, 1H), 3.30–2.96 (m, 5H), 1.98–1.43 (m, 9H), 1.40 (d, J = 7.2 Hz, 3H), 1.38–1.30 (m, 9H), 1.00–0.89 (m, 6H). MSI (ESI): 740 [$\text{M} + \text{H}$] $^+$, 371 [$\text{M} + 2\text{H}$] $^{2+}$. t_{R} = 3.02 min.

N-((8*S*,11*S*,14*S*,17*S*)-8-(((*S*)-1-Amino-3-hydroxy-1-oxopropan-2-yl)carbonyl)-3-ethyl-18-(furan-2-yl)-11-isobutyl-2,14-dimethyl-10,13,16-trioxo-3,9,12,15-tetraazaocadecan-17-yl)nicotinamide (UNC6382). The above general procedure yielded 3.3 mg (8.1%) of the title compound as a white solid. ^1H NMR (400 MHz, methanol- d_4) δ 8.99 (s, 1H), 8.73 (d, J = 5.1 Hz, 1H), 8.33–8.26 (m, 1H), 7.61 (dd, J = 8.0, 4.9 Hz, 1H), 7.44–7.39 (m, 1H), 6.35–6.29 (m, 1H), 6.25–6.20 (m, 1H), 4.42–4.27 (m, 4H), 3.89–3.75 (m, 2H), 3.74–3.64 (m, 1H), 3.29–2.96 (m, 6H), 1.98–1.44 (m, 9H), 1.38 (d, J = 7.2 Hz, 3H), 1.37–1.28 (m, 9H), 0.99–0.86 (m, 6H). MSI (ESI): 729 [$\text{M} + \text{H}$] $^+$, 365 [$\text{M} + 2\text{H}$] $^{2+}$. t_{R} = 3.72 min.

N-((8*S*,11*S*,14*S*,17*S*)-8-(((*S*)-1-Amino-3-hydroxy-1-oxopropan-2-yl)carbonyl)-18-cyclohexyl-3-ethyl-11-isobutyl-2,14-dimethyl-10,13,16-trioxo-3,9,12,15-tetraazaocadecan-17-yl)nicotinamide (UNC6383). The above general procedure yielded 3.5 mg (8.4%) of the title compound as a white solid. ^1H NMR (400 MHz, methanol- d_4) δ 9.09 (s, 1H), 8.76 (d, J = 4.2 Hz, 1H), 8.41 (dt, J = 8.0, 1.9 Hz, 1H), 7.65 (dd, J = 7.8, 5.2 Hz, 1H), 4.55 (dd, J = 9.3, 5.9 Hz, 1H), 4.41–4.28 (m,

4H), 3.88–3.76 (m, 2H), 3.74–3.65 (m, 1H), 3.29–2.97 (m, 4H), 2.03–1.42 (m, 18H), 1.39 (d, $J = 7.2$ Hz, 3H), 1.37–1.14 (m, 11H), 1.08–0.96 (m, 2H), 0.96–0.88 (m, 6H). MSI (ESI): 745 [M + H]⁺, 373 [M + 2H]²⁺. $t_R = 4.36$ min.

N-((8*S*,11*S*,14*S*,17*S*)-8-(((*S*)-1-Amino-3-hydroxy-1-oxopropan-2-yl)carbamoyl)-11-benzyl-3-ethyl-2,14-dimethyl-10,13,16-trioxo-18-phenyl-3,9,12,15-tetraazaoctadecan-17-yl)nicotinamide (UNC6384). The above general procedure yielded 7.5 mg (17%) of the title compound as a white solid. ¹H NMR (400 MHz, methanol-*d*₄) δ 8.93 (d, $J = 2.1$ Hz, 1H), 8.73 (dd, $J = 5.0, 1.6$ Hz, 1H), 8.29 (dt, $J = 8.0, 1.9$ Hz, 1H), 7.64 (dd, $J = 8.0, 5.1$ Hz, 1H), 7.34–7.12 (m, 10H), 4.79–4.75 (m, 1H), 4.54 (dd, $J = 9.3, 5.2$ Hz, 1H), 4.43–4.35 (m, 2H), 4.25 (q, $J = 7.2$ Hz, 1H), 3.87–3.75 (m, 2H), 3.71–3.62 (m, 1H), 3.26–2.95 (m, 8H), 1.98–1.39 (m, 6H), 1.37–1.23 (m, 12H). MSI (ESI): 773 [M + H]⁺, 387 [M + 2H]²⁺. $t_R = 4.00$ min.

N-((8*S*,11*S*,14*S*,17*S*)-8-(((*S*)-1-Amino-3-hydroxy-1-oxopropan-2-yl)carbamoyl)-3-ethyl-11-isobutyl-2,14-dimethyl-10,13,16-trioxo-18-phenyl-3,9,12,15-tetraazaoctadecan-17-yl)-4-(dimethylamino)benzamide (UNC6386). The above general procedure yielded 8.0 mg (18%) of the title compound as a white solid. ¹H NMR (400 MHz, methanol-*d*₄) δ 7.71 (d, $J = 8.9$ Hz, 2H), 7.35–7.27 (m, 4H), 7.26–7.19 (m, 1H), 6.77 (d, $J = 9.0$ Hz, 2H), 4.60–4.54 (m, 1H), 4.40–4.29 (m, 3H), 4.25 (q, $J = 7.1$ Hz, 1H), 3.86–3.73 (m, 2H), 3.67–3.57 (m, 1H), 3.29–3.05 (m, 5H), 3.04 (s, 6H), 3.01–2.90 (m, 1H), 1.98–1.42 (m, 9H), 1.38 (d, $J = 7.2$ Hz, 3H), 1.34–1.22 (m, 9H), 0.99–0.87 (m, 6H). MSI (ESI): 781 [M + H]⁺, 391 [M + 2H]²⁺. $t_R = 4.40$ min.

4-Amino-*N*-((8*S*,11*S*,14*S*,17*S*)-8-(((*S*)-1-amino-3-hydroxy-1-oxopropan-2-yl)carbamoyl)-3-ethyl-11-isobutyl-2,14-dimethyl-10,13,16-trioxo-18-phenyl-3,9,12,15-tetraazaoctadecan-17-yl)-3-bromobenzamide (UNC6387). The above general procedure yielded 19.7 mg (43.0%) of the title compound as a white solid. ¹H NMR (400 MHz, methanol-*d*₄) δ 7.91 (d, $J = 2.0$ Hz, 1H), 7.57 (dd, $J = 8.5, 2.1$ Hz, 1H), 7.35–7.18 (m, 5H), 6.80 (d, $J = 8.5$ Hz, 1H), 4.57–4.51 (m, 1H), 4.39–4.28 (m, 3H), 4.24 (q, $J = 7.2$ Hz, 1H), 3.86–3.72 (m, 2H), 3.68–3.56 (m, 1H), 3.28–2.88 (m, 6H), 2.00–1.42 (m, 9H), 1.38 (d, $J = 7.3$ Hz, 3H), 1.33–1.23 (m, 9H), 1.00–0.87 (m, 6H). MSI (ESI): 831/833 [M + H]⁺, 416 [M + 2H]²⁺. $t_R = 4.17$ min.

N-((8*S*,11*S*,14*S*,17*S*)-8-(((*S*)-1-Amino-3-hydroxy-1-oxopropan-2-yl)carbamoyl)-3-ethyl-11-isobutyl-2,14-dimethyl-10,13,16-trioxo-18-phenyl-3,9,12,15-tetraazaoctadecan-17-yl)furan-3-carboxamide (UNC6389). The above general procedure yielded 9.5 mg (23.3%) of the title compound as a white solid. ¹H NMR (400 MHz, methanol-*d*₄) δ 8.06 (s, 1H), 7.59–7.52 (m, 1H), 7.32–7.18 (m, 5H), 6.78 (s, 1H), 4.71–4.63 (m, 1H), 4.41–4.23 (m, 4H), 3.87–3.74 (m, 2H), 3.71–3.60 (m, 1H), 3.27–2.93 (m, 6H), 1.98–1.43 (m, 9H), 1.37 (d, $J = 7.2$ Hz, 3H), 1.35–1.27 (m, 9H), 0.98–0.89 (m, 6H). MSI (ESI): 728 [M + H]⁺, 364 [M + 2H]²⁺. $t_R = 4.11$ min.

N-((8*S*,11*S*,14*S*,17*S*)-8-(((*S*)-1-Amino-3-hydroxy-1-oxopropan-2-yl)carbamoyl)-3-ethyl-11-isobutyl-2,14-dimethyl-10,13,16-trioxo-18-phenyl-3,9,12,15-tetraazaoctadecan-17-yl)isoquinoline-7-carboxamide (UNC6390). The above general procedure yielded 4.7 mg (11%) of the title compound as a white solid. ¹H NMR (400 MHz, methanol-*d*₄) δ 9.60 (s, 1H), 8.60 (d, $J = 6.2$ Hz, 1H), 8.48 (s, 1H), 8.39 (d, $J = 8.7$ Hz, 1H), 8.26 (d, $J = 6.2$ Hz, 1H), 8.13 (d, $J = 8.6, 1.6$ Hz,

1H), 7.39–7.26 (m, 4H), 7.26–7.18 (m, 1H), 4.42–4.30 (m, 4H), 3.87–3.73 (m, 2H), 3.73–3.61 (m, 1H), 3.29–2.95 (m, 6H), 1.98–1.44 (m, 9H), 1.40 (d, $J = 7.2$ Hz, 3H), 1.35–1.27 (m, 9H), 0.96–0.89 (m, 6H). MSI (ESI): 789 [M + H]⁺, 395 [M + 2H]²⁺. $t_R = 4.27$ min.

N-((8*S*,11*S*,14*S*,17*S*)-8-(((*S*)-1-Amino-3-hydroxy-1-oxopropan-2-yl)carbamoyl)-3-ethyl-11-isobutyl-2,14-dimethyl-10,13,16-trioxo-18-phenyl-3,9,12,15-tetraazaoctadecan-17-yl)quinoline-6-carboxamide (UNC6391). The above general procedure yielded 9.1 mg (21%) of the title compound as a white solid. ¹H NMR (400 MHz, methanol-*d*₄) δ 9.05 (d, $J = 4.7, 1.6$ Hz, 1H), 8.66 (d, $J = 8.2$ Hz, 1H), 8.49 (s, 1H), 8.14 (d, $J = 8.6$ Hz, 1H), 8.02 (d, $J = 8.7, 1.7$ Hz, 1H), 7.82–7.75 (m, 1H), 7.39–7.26 (m, 4H), 7.26–7.18 (m, 1H), 4.42–4.29 (m, 4H), 3.88–3.74 (m, 2H), 3.69–3.59 (m, 1H), 3.27–2.94 (m, 6H), 1.98–1.44 (m, 9H), 1.41 (d, $J = 7.2$ Hz, 3H), 1.35–1.25 (m, 9H), 0.96–0.88 (m, 6H). MSI (ESI): 789 [M + H]⁺, 395 [M + 2H]²⁺. $t_R = 4.06$ min.

N-((8*S*,11*S*,14*S*,17*S*)-8-(((*S*)-1-Amino-3-hydroxy-1-oxopropan-2-yl)carbamoyl)-11-(3,4-dimethoxybenzyl)-3-ethyl-2,14-dimethyl-10,13,16-trioxo-18-phenyl-3,9,12,15-tetraazaoctadecan-17-yl)nicotinamide (UNC6392). The above general procedure yielded 6.9 mg (15%) of the title compound as a white solid. ¹H NMR (400 MHz, methanol-*d*₄) δ 8.96–8.91 (m, 1H), 8.74 (d, $J = 5.2, 1.6$ Hz, 1H), 8.31 (dt, $J = 8.2, 1.8$ Hz, 1H), 7.66 (dd, $J = 8.0, 5.3$ Hz, 1H), 7.32–7.15 (m, 5H), 6.89–6.75 (m, 3H), 4.81–4.76 (m, 1H), 4.57–4.49 (m, 1H), 4.42–4.34 (m, 2H), 4.29 (q, $J = 7.1$ Hz, 1H), 3.86–3.71 (m, 8H), 3.71–3.62 (m, 1H), 3.28–2.94 (m, 8H), 1.97–1.37 (m, 6H), 1.37–1.27 (m, 12H). MSI (ESI): 833 [M + H]⁺, 417 [M + 2H]²⁺. $t_R = 3.90$ min.

4-Amino-*N*-((8*S*,11*S*,14*S*,17*S*)-8-(((*S*)-1-amino-3-hydroxy-1-oxopropan-2-yl)carbamoyl)-3-ethyl-11-isobutyl-2,14-dimethyl-10,13,16-trioxo-18-phenyl-3,9,12,15-tetraazaoctadecan-17-yl)benzamide (UNC6393). The above general procedure yielded 10.0 mg (24.0%) of the title compound as a white solid. ¹H NMR (400 MHz, methanol-*d*₄) δ 7.69–7.61 (m, 2H), 7.36–7.19 (m, 5H), 6.80 (dd, $J = 20.9, 8.4$ Hz, 2H), 4.61–4.20 (m, 5H), 3.88–3.70 (m, 2H), 3.69–3.51 (m, 1H), 3.28–2.88 (m, 6H), 1.98–1.43 (m, 9H), 1.38 (d, $J = 7.1$ Hz, 3H), 1.35–1.16 (m, 9H), 0.98–0.87 (m, 6H). MSI (ESI): 753 [M + H]⁺, 377 [M + 2H]²⁺. $t_R = 3.88$ min.

N-((8*S*,11*S*,14*S*,17*S*)-8-(((*S*)-1-Amino-3-hydroxy-1-oxopropan-2-yl)carbamoyl)-3-ethyl-11-isobutyl-2,14-dimethyl-10,13,16-trioxo-18-phenyl-3,9,12,15-tetraazaoctadecan-17-yl)-4-(methylamino)benzamide (UNC6394). The above general procedure yielded 9.1 mg (21%) of the title compound as a white solid. ¹H NMR (400 MHz, methanol-*d*₄) δ 7.65 (d, $J = 8.7$ Hz, 2H), 7.36–7.19 (m, 5H), 6.61 (d, $J = 8.7$ Hz, 2H), 4.58–4.49 (m, 1H), 4.39–4.19 (m, 4H), 3.86–3.73 (m, 2H), 3.65–3.55 (m, 1H), 3.28–2.88 (m, 6H), 2.82 (s, 3H), 1.98–1.40 (m, 9H), 1.38 (d, $J = 7.3$ Hz, 3H), 1.34–1.16 (m, 9H), 0.98–0.87 (m, 6H). MSI (ESI): 767 [M + H]⁺, 384 [M + 2H]²⁺. $t_R = 4.21$ min.

4-Amino-*N*-((8*S*,11*S*,14*S*,17*S*)-8-(((*S*)-1-Amino-3-hydroxy-1-oxopropan-2-yl)carbamoyl)-3-ethyl-11-isobutyl-2,14-dimethyl-10,13,16-trioxo-18-phenyl-3,9,12,15-tetraazaoctadecan-17-yl)cyclohexane-1-carboxamide (UNC6865). The above general procedure yielded 7.9 mg (16%) of the title compound as a white solid. ¹H NMR (400 MHz, methanol-*d*₄) δ 7.30–7.24 (m, 4H), 7.23–7.18 (m, 1H), 4.65–4.59 (m, 1H), 4.41–4.30 (m, 4H), 3.88–3.75 (m, 2H), 3.73–3.64 (m, 1H), 3.29–2.96 (m, 6H), 2.87 (dd, $J = 14.0, 10.3$ Hz, 1H), 2.48–

2.41 (m, 1H), 1.99–1.42 (m, 17H), 1.38 (d, $J = 7.1$ Hz, 3H), 1.36–1.30 (m, 9H), 1.00–0.91 (m, 6H). MSI (ESI): 759 [M + H]⁺, 380 [M + 2H]²⁺. $t_R = 0.60$ min.

N-((8S,11S,14S,17S)-8-(((S)-1-Amino-3-hydroxy-1-oxopropan-2-yl)carbamoyl)-3-ethyl-11-isobutyl-2,14-dimethyl-10,13,16-trioxo-18-phenyl-3,9,12,15-tetraazaoctadecan-17-yl)-4-(aminomethyl)cyclohexane-1-carboxamide (UNC6866). The above general procedure yielded 4.7 mg (9.6%) of the title compound as a white solid. ¹H NMR (400 MHz, methanol-*d*₄) δ 7.30–7.18 (m, 5H), 4.61–4.55 (m, 1H), 4.41–4.26 (m, 3H), 3.87–3.74 (m, 2H), 3.74–3.62 (m, 1H), 3.28–2.95 (m, 6H), 2.90 (dd, $J = 14.1, 9.7$ Hz, 1H), 2.77 (d, $J = 7.0$ Hz, 2H), 2.25–2.14 (m, 1H), 2.01–1.39 (m, 15H), 1.38–1.24 (m, 13H), 1.11–1.00 (m, 2H), 1.00–0.91 (m, 6H). MSI (ESI): 773 [M + H]⁺, 387 [M + 2H]²⁺. $t_R = 0.59$ min.

N-((8S,11S,14S,17S)-8-(((S)-1-Amino-3-hydroxy-1-oxopropan-2-yl)carbamoyl)-3-ethyl-11-isobutyl-2,14-dimethyl-10,13,16-trioxo-18-phenyl-3,9,12,15-tetraazaoctadecan-17-yl)isonicotinamide (UNC6867). The above general procedure yielded 21.4 mg (69.0%) of the title compound as a white solid. ¹H NMR (400 MHz, methanol-*d*₄) δ 8.78 (d, $J = 6.3$ Hz, 2H), 7.93–7.88 (m, 2H), 7.34–7.25 (m, 4H), 7.24–7.18 (m, 1H), 4.87–4.81 (m, 1H), 4.41–4.31 (m, 4H), 3.87–3.75 (m, 2H), 3.72–3.63 (m, 1H), 3.30–2.95 (m, 6H), 2.00–1.43 (m, 9H), 1.39 (d, $J = 7.2$ Hz, 3H), 1.36–1.28 (m, 9H), 0.98–0.89 (m, 6H). MSI (ESI): 739 [M + H]⁺, 370 [M + 2H]²⁺. $t_R = 2.56$ min.

3-Amino-N-((8S,11S,14S,17S)-8-(((S)-1-amino-3-hydroxy-1-oxopropan-2-yl)carbamoyl)-3-ethyl-11-isobutyl-2,14-dimethyl-10,13,16-trioxo-18-phenyl-3,9,12,15-tetraazaoctadecan-17-yl)-4-bromobenzamide (UNC6868). The above general procedure yielded 15.8 mg (45.3%) of the title compound as a white solid. ¹H NMR (400 MHz, methanol-*d*₄) δ 7.43 (d, $J = 8.3$ Hz, 1H), 7.33–7.26 (m, 4H), 7.25–7.20 (m, 1H), 7.19 (d, $J = 2.1$ Hz, 1H), 6.92 (dd, $J = 8.3, 2.1$ Hz, 1H), 4.71–4.64 (m, 1H), 4.40–4.26 (m, 4H), 3.87–3.74 (m, 2H), 3.68–3.60 (m, 1H), 3.28–2.91 (m, 6H), 1.98–1.42 (m, 9H), 1.38 (d, $J = 7.2$ Hz, 3H), 1.34–1.26 (m, 9H), 0.99–0.87 (m, 6H). MSI (ESI): 831/833 [M + H]⁺, 416 [M + 2H]²⁺. $t_R = 3.01$ min.

3-Amino-N-((8S,11S,14S,17S)-8-(((S)-1-amino-3-hydroxy-1-oxopropan-2-yl)carbamoyl)-18-cyclohexyl-11-(3,4-dimethoxybenzyl)-3-ethyl-2,14-dimethyl-10,13,16-trioxo-3,9,12,15-tetraazaoctadecan-17-yl)-4-bromobenzamide (UNC7047). The above general procedure yielded 11.7 mg (27.6%) of the title compound as a white solid. ¹H NMR (400 MHz, methanol-*d*₄) δ 7.48 (d, $J = 8.3$ Hz, 1H), 7.33 (d, $J = 2.1$ Hz, 1H), 7.06 (dd, $J = 8.3, 2.1$ Hz, 1H), 6.81–6.76 (m, 2H), 6.72 (dd, $J = 8.2, 1.7$ Hz, 1H), 4.55–4.50 (m, 1H), 4.48–4.42 (m, 1H), 4.40–4.34 (m, 2H), 4.22 (q, $J = 7.1$ Hz, 1H), 3.88–3.61 (m, 9H), 3.27–2.92 (m, 6H), 1.99–1.12 (m, 29H), 1.05–0.88 (m, 2H). MSI (ESI): 931/933 [M + H]⁺, 466 [M + 2H]²⁺. $t_R = 3.28$ min.

4-Amino-N-((8S,11S,14S,17S)-8-(((S)-1-amino-3-hydroxy-1-oxopropan-2-yl)carbamoyl)-18-cyclohexyl-11-(3,4-dimethoxybenzyl)-3-ethyl-2,14-dimethyl-10,13,16-trioxo-3,9,12,15-tetraazaoctadecan-17-yl)-3-bromobenzamide (UNC7048). The above general procedure yielded 11.0 mg (26.0%) of the title compound as a white solid. ¹H NMR (400 MHz, methanol-*d*₄) δ 8.08 (d, $J = 2.0$ Hz, 1H), 7.72 (dd, $J = 8.5, 2.0$ Hz, 1H), 6.84 (d, $J = 8.5$ Hz, 1H), 6.79–6.69 (m, 3H), 4.54–4.48 (m, 1H), 4.41–4.34 (m, 3H), 4.16 (q, $J = 7.3$ Hz, 1H), 3.88–3.59 (m, 9H), 3.26–2.92 (m, 6H), 2.02–1.11 (m,

29H), 1.05–0.90 (m, 2H). MSI (ESI): 931/933 [M + H]⁺, 466 [M + 2H]²⁺. $t_R = 3.20$ min.

3-Amino-N-((8S,11S,14S,17S)-8-(((S)-1-amino-3-hydroxy-1-oxopropan-2-yl)carbamoyl)-18-cyclohexyl-11-(3,4-dimethoxybenzyl)-3-ethyl-2,14-dimethyl-10,13,16-trioxo-3,9,12,15-tetraazaoctadecan-17-yl)-4-fluorobenzamide (UNC7049). The above general procedure yielded 9.8 mg (24.6%) of the title compound as a white solid. ¹H NMR (400 MHz, methanol-*d*₄) δ 7.40 (dd, $J = 8.4, 2.1$ Hz, 1H), 7.25–7.20 (m, 1H), 7.07 (dd, $J = 10.9, 8.5$ Hz, 1H), 6.82–6.77 (m, 2H), 6.75–6.70 (m, 1H), 4.54–4.49 (m, 1H), 4.48–4.42 (m, 1H), 4.40–4.33 (m, 2H), 4.22 (q, $J = 7.2$ Hz, 1H), 3.88–3.61 (m, 9H), 3.28–2.93 (m, 6H), 1.99–1.12 (m, 29H), 1.05–0.88 (m, 2H). MSI (ESI): 871 [M + H]⁺, 436 [M + 2H]²⁺. $t_R = 3.11$ min.

4-Amino-N-((8S,11S,14S,17S)-8-(((S)-1-amino-3-hydroxy-1-oxopropan-2-yl)carbamoyl)-18-cyclohexyl-11-(3,4-dimethoxybenzyl)-3-ethyl-2,14-dimethyl-10,13,16-trioxo-3,9,12,15-tetraazaoctadecan-17-yl)-3-fluorobenzamide (UNC7050). The above general procedure yielded 10.0 mg (25.1%) of the title compound as a white solid. ¹H NMR (400 MHz, methanol-*d*₄) δ 7.65–7.56 (m, 2H), 6.84 (t, $J = 8.6$ Hz, 1H), 6.80–6.69 (m, 3H), 4.54–4.48 (m, 1H), 4.42–4.34 (m, 3H), 4.18 (q, $J = 7.2$ Hz, 1H), 3.88–3.61 (m, 9H), 3.27–2.92 (m, 6H), 2.02–1.12 (m, 29H), 1.06–0.89 (m, 2H). MSI (ESI): 871 [M + H]⁺, 436 [M + 2H]²⁺. $t_R = 3.08$ min.

On-Bead Screening Protocol for the OBOC Library.

On-bead library screening was conducted as described previously.⁵⁶ Both of the synthesized sub-libraries were equilibrated, separately, in 25 mM Tris, pH 7.8, 150 mM NaCl, and 0.1% Tween-20 (TBST) overnight. All of the traditional six-residue sub-library was equilibrated in 12 mL TBST in a 15 mL conical tube, and approximately 1/3 of the five-residue fused cap sub-library was equilibrated in 1.5 mL TBST in a 2.0 mL Eppendorf tube. Individual magnetic screens follow a similar protocol to that originally described by Astle et al.⁶⁵ For 1 h, the resin beads were blocked in 5% BSA in TBST using the listed volumes above at RT. The resin from each sub-library was washed once and then incubated with 2 μ M His-tagged CBX5 in 2.5% BSA in TBST at appropriate volumes for 1 h. Simultaneously, mouse anti-His antibody (13 μ L of a 1 μ g/ μ L solution; Pierce MA1–21315) was incubated with Protein G Dynabeads (65 μ L; Life Technologies) in 2.5% BSA in TBST (500 μ L). After incubation, the Dynabeads were washed 3 \times 500 μ L in TBST, and the resin of the two sub-libraries was washed 3 \times 12 mL (six-residue) or 3 \times 1.5 mL (five-residue) in TBST. A 2.5% BSA in TBST was added to each sub-library at appropriate volumes. After resuspension of Dynabeads in 500 μ L of 2.5% BSA in TBST, 428 μ L was added to the six-residue sub-library and 72 μ L was added to the five-residue sub-library. The library beads and magnetic beads were left to mix at RT for 1 h. A magnet was used to remove CBX5 hits and non-specific binders. As no hits were present for the five-residue fused cap sub-library, screening was discontinued for this aliquot. The remaining six-residue sub-library was pooled into one 2.0 mL Eppendorf tube, cleared of remaining unconjugated Dynabeads, and incubated with 10 μ M UNC4869 as a soluble competitor in 1.0 mL of 2.5% BSA in TBST. At 1 and 3 h, the beads were subjected to a magnet, and de-magnetized beads were removed and pooled so that hit compounds were separated across three aliquots (<1, <3, and >3 h magnetization). The <3 and >3 h aliquots were washed 1 \times 500 μ L in TBST and then stripped in 1.0 mL of 1% SDS

overnight at RT. Resin beads were then washed $1 \times \text{H}_2\text{O}$, $1 \times 1 \text{ M NaCl}$, and $6 \times \text{TBST}$ prior to cross-screening. Negative selection screens with the two aliquots of CBX5 hit beads were then performed with $2 \mu\text{M}$ His-CBX7 and $2 \mu\text{M}$ His-MPP8 under the same conditions but with the following modifications: screening volumes were adjusted to 1.5 mL, and $2 \mu\text{L}$ of anti-His antibody was pre-incubated with $10 \mu\text{L}$ of Protein G Dynabeads in $100 \mu\text{L}$ 2.5% BSA in TBST. These negative selections were done sequentially, and after each screen, the magnetized and un-magnetized resin beads were isolated, stripped of protein by SDS treatment, and stringently washed before proceeding to the next negative selection. After both negative selections, the CBX5-selective beads from both <3 and >3 h magnetization aliquots were rinsed repeatedly in ethanol and then equilibrated overnight in ethanol prior to cyanogen bromide cleavage.

Hit Cleavage and MALDI-TOF/TOF Identification of Compounds from the OBOC Library. Cleavage and identification of compounds was conducted as described previously.⁵⁶ The hit beads were isolated (1 bead per well) into a 96-well plate (Thermo Scientific 0.2 mL 96-well PCR plate). The ethanol solutions were left to evaporate. Cyanogen bromide cleavage followed previously described protocols.^{65,66}

In brief, a mixture of 0.25 M cyanogen bromide in 10% water, 40% acetic acid, and 50% acetonitrile was prepared. A total of $20 \mu\text{L}$ of this mixture was added to each well. The plates were loosely covered and left to mix overnight on a shaker platform at room temperature in a fume hood. Cleaved compounds were redissolved in $10 \mu\text{L}$ of 1:1 water:acetonitrile. From this solution, $0.5 \mu\text{L}$ was spotted on an Opti-TOF 384-well MALDI plate and $0.5 \mu\text{L}$ of a saturated solution of α -cyano-4-hydroxycinnamic acid in 50% acetonitrile and 50% water with 0.1% TFA was spotted on top. The solutions were left to evaporate. Spectra were recorded on an ABSciex 5800 MALDI-TOF/TOF in positive, linear mode with a laser power between 2200 and 2600.

Protein Expression and Purification. *Expression Constructs.* The chromodomains of CBX2 (residues 9–66 of NP_005180), CBX4 (residues 8–65 of NP_003646), CBX6 (residues 8–65 of NP_055107), CBX7 (residues 8–62 of NP_783640 and CDYL2 (residues 1–75 of NP_689555) were expressed with C-terminal His-tags in pET30 expression vectors. The chromodomain of CBX8 (residues 8–61 of NP_065700) was expressed with an N-terminal His-tag in a pET28 expression vector. The chromodomains of CBX5 (residues 18–75 of NP_036429) and MPP8 (residues 55–116 of NP_059990) were expressed with N-terminal His-tags in pET28 expression vectors.

Protein Expression and Purification. All expression constructs were transformed into Rosetta BL21(DE3)pLysS competent cells (Novagen, EMD Chemicals, San Diego, CA). Protein expression was induced by growing cells at 37°C with shaking until the OD600 reached ~ 0.6 – 0.8 at which time the temperature was lowered to 18°C and expression was induced by adding 0.5 mM IPTG and continuing shaking overnight. Cells were harvested by centrifugation, and pellets were stored at -80°C .

His-tagged proteins were purified by re-suspending thawed cell pellets in 30 mL of lysis buffer (50 mM sodium phosphate pH 7.2, 50 mM NaCl, 30 mM imidazole, $1 \times$ EDTA free protease inhibitor cocktail (Roche Diagnostics, Indianapolis, IN)) per liter of culture. Cells were lysed on ice by sonication with a Branson Digital 450 Sonifier (Branson Ultrasonics,

Danbury, CT) at 40% amplitude for 12 cycles with each cycle consisting of a 20 s pulse followed by a 40 s rest. The cell lysate was clarified by centrifugation and loaded onto a HisTrap FF column (GE Healthcare, Piscataway, NJ) that had been pre-equilibrated with 10 column volumes of binding buffer (50 mM sodium phosphate, pH 7.2, 500 mM NaCl, 30 mM imidazole) using an AKTA FPLC (GE Healthcare, Piscataway, NJ). The column was washed with 15 column volumes of binding buffer, and protein was eluted in a linear gradient to 100% elution buffer (50 mM sodium phosphate, pH 7.2, 500 mM NaCl, 500 mM imidazole) over 20 column volumes. Peak fractions containing the desired protein were pooled and concentrated to 2 mL in Amicon Ultra-15 concentrators 3000 molecular weight cut-off (Merck Millipore, Carrigtwohill Co. Cork IRL). Concentrated protein was loaded onto a HiLoad 26/60 Superdex 75 prep grade column (GE Healthcare, Piscataway, NJ) that had been pre-equilibrated with 1.2 column volumes of sizing buffer (25 mM Tris, pH 7.5, 250 mM NaCl, 2 mM DTT, 5% glycerol) using an ATKA Purifier (GE Healthcare, Piscataway, NJ). Protein was eluted isocratically in sizing buffer over 1.3 column volumes at a flow rate of 2 mL/min collecting 3 mL fractions. Peak fractions were analyzed for purity by SDS-PAGE, and those containing pure protein were pooled and concentrated using Amicon Ultra-15 concentrators with 3000 molecular weight cut-off (Merck Millipore, Carrigtwohill Co. Cork IRL). Protein was exchanged into a buffer containing 25 mM Tris, pH 7.5, 150 mM NaCl, and 2 mM β -mercaptoethanol before use in ITC.

Differential Scanning Fluorimetry (DSF) Assay for CBX5. DSF experiments were performed using an Applied Biosystems ViiA 7 Real-Time PCR System. Assays were completed using DSF buffer containing 25 mM Tris pH 7.5 and 50 mM NaCl. Clear, DNase/RNase free, polypropylene 384-well PCR plates (Genesee Scientific, cat. #: 24-305) were used for screening. 384-well, V-bottom polypropylene plates (Greiner, #781280) were used as mother plates for compound dilutions and transfer of assay mixtures. Concentrated DMSO stocks (10 mM) of all test compounds were used to make dilutions in assay buffer to either 1.0 (10% DMSO) or 2.0 mM (20% DMSO) on the mother plate. Test compounds were then dispensed at both concentrations onto PCR assay plates at a volume of $2.0 \mu\text{L}$ using an E-1 ClipTip 8-channel 1–125 μL 384-well pipette (ThermoFisher; P4672060). Protein (31.3 μM CBX5) and SYPRO Orange Dye (Invitrogen no. S6650; diluted from 5000X to 12.5X) were added together and gently mixed by pipetting. A total of $8.0 \mu\text{L}$ of the protein and dye mixture was then added to each well of an assay ready plate using the E-1 ClipTip pipette to yield final assay component concentrations of 25 μM CBX5, 10X SYPRO Orange Dye, and either 200 μM (2.0% DMSO) or 400 μM (4.0% DMSO) test compound at $10 \mu\text{L}$ of final volume. Following the addition of all assay components, plates were sealed with clear covers and centrifuged at $1000 \times g$ for 2 min. Thermal denaturation was achieved by applying a temperature ramp from 25 to 99°C ($0.05^\circ\text{C}/\text{s}$) with fluorescence readings every 0.25°C . Data analysis was completed using Applied Biosystems Protein Thermal Shift software and GraphPad Prism 8.

Time-Resolved Fluorescence Resonance Energy Transfer (TR-FRET) Assay Protocol. The TR-FRET assay was performed as described in Rectenwald et al.⁶² A stock solution of $10 \times$ Kme reader buffer (200 mM Tris pH 7.5, 1500 mM NaCl, and 0.5% Tween 20) was prepared, $0.2 \mu\text{m}$ filtered, stored at room temperature, and was used throughout. Assays

were completed using freshly made Kme reader buffer containing 20 mM Tris pH 7.5, 150 mM NaCl, 0.05% Tween 20, and 2 mM dithiothreitol (DTT). White, low-volume, flat-bottom, non-binding, 384-well microplates (Greiner, #784904) were used for screening with a total assay volume of 10 μ L. 384-well, V-bottom polypropylene plates (Greiner, #781280) were used as mother plates for compound serial dilutions and for transfer of assay mixtures. Concentrated DMSO stocks (10 mM) of all test compounds were used to make serial dilutions in DMSO. Test compounds were then dispensed across the mother plate at 100 \times final concentration in columns 3–22 using a TECAN Freedom EVO liquid handling work station. Using a TTP Labtech Mosquito HTS liquid handling instrument, assay ready plates were stamped by adding 100 nL of either control compound into columns 1 and 2, test compounds from the mother plate into columns 3–22, or DMSO into columns 23 and 24. Protein (CBX2 assay: 15 nM, CBX4 assay: 5 nM, CBX6 assay: 5 nM, CBX7 assay: 1 nM, CBX8 assay: 10 nM, CBX5 assay: 30 nM, MPP8 assay: 25 nM, CDYL2 assay: 1 nM), biotinylated tracer ligand (CBX2 assay: 30 nM UNC4195, CBX4 assay: 10 nM UNC4195, CBX6 assay: 10 nM UNC4195, CBX7 assay: 5 nM UNC4195, CBX8 assay: 20 nM UNC4195, CBX5 assay: 30 nM P42, MPP8 assay: 50 nM P42, CDYL2 assay: 8 nM biotin-UNC4848), and the TR-FRET reagents (PerkinElmer LANCE Ultra ULight-anti-6xHis at 10 nM and PerkinElmer LANCE Eu-W1024 Streptavidin at 2 nM) were added together at a final volume of 6.00 mL per individual 384-well assay plate and gently mixed by pipetting and rocking. A total of 10 μ L of the assay mixture was then added to each well of an assay ready plate using a Multidrop Combi (ThermoFisher). Following the addition of all assay components, plates were sealed with clear covers, gently mixed on a tabletop shaker for 1 min, centrifuged at 1000 \times g for 2 min, and allowed to equilibrate in a dark space for 1 h before reading. Measurements were taken on an EnVision 2103 Multilabel Plate Reader (Perkin Elmer) using an excitation filter at 320 nm and emission filters at 615 and 665 nm. The 615 nm and 650 nm emission signals were measured simultaneously using a dual mirror at D400/D630. TR-FRET output signal was expressed as emission ratios of acceptor/donor (665/615 nm) counts. Percent inhibition was calculated on a scale of 0% (i.e., activity with DMSO vehicle only) to 100% (100 μ M UNC4976 (CBX2, CBX4, CBX6, CBX7, and CBX8), 100 μ M UNC5241 (CBX5 and MPP8), or 100 μ M UNC4848 using full column controls on each plate. The interquartile mean of control wells was used to calculate Z' values. For dose–response curves, data was fit with a four-parameter nonlinear regression analysis using ScreenAble software to obtain IC_{50} values.

Isothermal Titration Calorimetry (ITC) Experiments.

All ITC measurements were recorded at 25 $^{\circ}$ C with an Auto-iTC200 isothermal titration calorimeter (MicroCal Inc., USA). All protein and compound stock samples were stored in ITC buffer (25 mM Tris–HCl, pH 7.5, 150 mM NaCl, and 2 mM β -mercaptoethanol) and then diluted to achieve the desired concentrations. Typically, either 50 μ M protein and 0.5 mM compound or 100 μ M and 1.0 mM compound were used; variations in these concentrations always maintained a 10:1 compound to protein ratio for all ITC experiments. The concentration of the protein stock solution was established using the Edelhoch method, whereas compound stock solutions were prepared based on mass. A typical experiment included a single 0.2 μ L compound injection into a 200 μ L cell

filled with protein followed by 26 subsequent 1.5 μ L injections of the compound. Injections were performed with a spacing of 180 s and a reference power of 8 cal/s. The initial data point was routinely deleted. The titration data was analyzed using Origin 7 Software (MicroCal Inc., USA) by the nonlinear least-squares method, fitting the heats of binding as a function of the compound to protein ratio to a one site binding model.

Chemiprecipitation from HEK293T Lysates with UNC7565. HEK293T cells were cultured in T175 or T225 tissue culture flasks until reaching 80–90% confluency. Following trypsinization and centrifugation, the cell pellet was washed twice with 1 \times PBS and either flash frozen in LN₂ and stored at –80 $^{\circ}$ C, or lysed for immediate use. Lysis was completed in Cytobuster Protein Extraction Reagent (EMD Millipore, 71,009) supplemented with 1 \times protease inhibitors (Roche) and Benzonase (25 U/mL final concentration, Novogen 70,746); the cell pellet was resuspended to a total volume of 500 μ L lysis solution. Samples were incubated at 37 $^{\circ}$ C for 10 min and then at RT for 20 min on an end-to-end rotator. Samples were then centrifuged at RT at 14,000 RPM for 30 s, and the supernatant was collected and transferred to a clean Eppendorf tube. Protein concentration was quantified by the Bradford protein assay. M-270 Streptavidin Dynabeads (Invitrogen) were used to immobilize biotinylated compounds for pulldowns. Prior to use, Dynabeads were washed 3 \times 500 μ L in TBST (20 mM Tris–HCl, pH 7.0, 150 mM NaCl, 0.1% Tween-20). UNC7565 was then immobilized by rotating 30 μ L of beads with a 20-fold excess of pulldown reagent, diluted to 150 μ L in TBST, at RT for 30 min on an end-to-end rotator. The unbound pulldown reagent was then removed by washing the Dynabeads with 3 \times 500 μ L of TBST. HEK293T lysate, at 1000 μ g protein per sample, was then transferred to an Eppendorf tube containing 30 μ L of Dynabeads that had been pre-bound to UNC7565, and the mixture was diluted to a final volume of 500 μ L in TBST. Samples were incubated overnight at 4 $^{\circ}$ C on an end-to-end rotator. The following morning, the depleted lysate was removed and the beads were washed with 3 \times 500 μ L of TBST. Beads were then resuspended with 30 μ L of MilliQ water/2 \times Laemmli sample buffer (BioRad, #1610737) (1:1) and heated at 95 $^{\circ}$ C for 3 min. Samples were then loaded into a BioRad Any kD Mini-PROTEAN TGX Stain-Free gel (12 well: #4569035, 15 well: #4569036) in BioRad 1 \times Tris/Glycine/SDS buffer (#1610772). Input samples used for western blotting were 1% of final protein concentration. Gels were run at RT for 30–40 min at 200 V. Transfer was completed onto a PVDF membrane in 1 \times Tris/Glycine buffer (#1610771) at 4 $^{\circ}$ C for 1 h at 100 V. Membranes were blocked for 45–60 min in Odyssey TBS blocking buffer (P/N: 927–50,000) and then incubated in TBST supplemented with the appropriate primary antibody overnight at 4 $^{\circ}$ C on a plate rocker. The following morning, membranes were washed with 3 \times TBST and incubated in TBST supplemented with the appropriate fluorescently labeled secondary antibody at RT for 1 h. Primary antibodies in this study include CBX1 (Abcam, ab10811, 1:1000), CBX3 (Millipore, EMD-05-690, 1:1000), CBX5 (Abcam, ab109028, 1:1000), CBX7 (Abcam, ab21873, 1:5000), MPP8 (Proteintech, 16796-1-AP, 1:1000), and SENP7 (Bethyl, A302-995A). Secondary antibodies in this study were infrared labeled antibodies (LI-COR, #926-32211 and #926-68070, 1:10,000), and blots were imaged on an LI-COR Odyssey imager.

■ ASSOCIATED CONTENT

SI Supporting Information

The Supporting Information is available free of charge at <https://pubs.acs.org/doi/10.1021/acsomega.1c05381>.

OBOC Screening Cascade, representative ITC curves, TR-FRET data, uncropped western blots, synthetic schemes, and HPLC and ¹H NMR spectra of intermediate and final compounds (PDF)

■ AUTHOR INFORMATION

Corresponding Author

Stephen V. Frye – *Center for Integrative Chemical Biology and Drug Discovery, Division of Chemical Biology and Medicinal Chemistry, UNC Eshelman School of Pharmacy, University of North Carolina at Chapel Hill, Chapel Hill, North Carolina 27599, United States*; orcid.org/0000-0002-2415-2215; Email: svfrye@email.unc.edu

Authors

Kelsey N. Lamb – *Center for Integrative Chemical Biology and Drug Discovery, Division of Chemical Biology and Medicinal Chemistry, UNC Eshelman School of Pharmacy, University of North Carolina at Chapel Hill, Chapel Hill, North Carolina 27599, United States*; Present Address: Vividion Therapeutics, 5820 Nancy Ridge Drive, San Diego, California 92121, United States (K.N.L.)

Sarah N. Dishman – *Center for Integrative Chemical Biology and Drug Discovery, Division of Chemical Biology and Medicinal Chemistry, UNC Eshelman School of Pharmacy, University of North Carolina at Chapel Hill, Chapel Hill, North Carolina 27599, United States*; Present Address: Department of Chemistry, University of California, One Shields Avenue, Davis, California 95616, United States (S.N.D.).

Jarod M. Waybright – *Center for Integrative Chemical Biology and Drug Discovery, Division of Chemical Biology and Medicinal Chemistry, UNC Eshelman School of Pharmacy, University of North Carolina at Chapel Hill, Chapel Hill, North Carolina 27599, United States*; Present Address: Design Therapeutics, 6055 Hidden Valley Road Suite 110, Carlsbad, California 92011, United States (J.M.W.); orcid.org/0000-0002-5226-8231

Isabelle A. Engelberg – *Center for Integrative Chemical Biology and Drug Discovery, Division of Chemical Biology and Medicinal Chemistry, UNC Eshelman School of Pharmacy, University of North Carolina at Chapel Hill, Chapel Hill, North Carolina 27599, United States*

Justin M. Rectenwald – *Center for Integrative Chemical Biology and Drug Discovery, Division of Chemical Biology and Medicinal Chemistry, UNC Eshelman School of Pharmacy, University of North Carolina at Chapel Hill, Chapel Hill, North Carolina 27599, United States*; Present Address: KBI Biopharma, 1101 Hamlin Road, Durham, NC 27704, United States (J.M.R.).

Jacqueline L. Norris-Drouin – *Center for Integrative Chemical Biology and Drug Discovery, Division of Chemical Biology and Medicinal Chemistry, UNC Eshelman School of Pharmacy, University of North Carolina at Chapel Hill, Chapel Hill, North Carolina 27599, United States*

Stephanie H. Cholensky – *Center for Integrative Chemical Biology and Drug Discovery, Division of Chemical Biology and Medicinal Chemistry, UNC Eshelman School of*

Pharmacy, University of North Carolina at Chapel Hill, Chapel Hill, North Carolina 27599, United States; Present Address: University of Minnesota, Lab: 4-108 Nils Hasselmo Hall, 312 Church Street, Minneapolis, Minnesota 55455, United States (S.H.C.).

Kenneth H. Pearce – *Center for Integrative Chemical Biology and Drug Discovery, Division of Chemical Biology and Medicinal Chemistry, UNC Eshelman School of Pharmacy, University of North Carolina at Chapel Hill, Chapel Hill, North Carolina 27599, United States*

Lindsey I. James – *Center for Integrative Chemical Biology and Drug Discovery, Division of Chemical Biology and Medicinal Chemistry, UNC Eshelman School of Pharmacy, University of North Carolina at Chapel Hill, Chapel Hill, North Carolina 27599, United States*; orcid.org/0000-0002-6034-7116

Complete contact information is available at: <https://pubs.acs.org/doi/10.1021/acsomega.1c05381>

Author Contributions

K.N.L., L.I.J., and S.V.F. developed the concept and designed the study. K.N.L. did combinatorial peptide synthesis and on bead screening. S.N.D. did follow-up peptidomimetic synthesis. K.N.L., I.A.E., and J.M.R. conducted TR-FRET under the guidance of K.H.P., K.N.L., and J.M.W. did ITC analysis. J.M.W. performed lysate pulldown experiments. J.L.N. and S.H.C. carried out protein preparation. K.N.L., L.I.J., and S.V.F. analyzed the data and wrote the manuscript. All authors have given approval to the final version of the manuscript.

Notes

The authors declare no competing financial interest.

■ ACKNOWLEDGMENTS

This work was supported by the National Institute of General Medical Sciences, US NIH (grant R01GM100919), to S.V.F. by the National Cancer Institute NIH (grant R01CA218392) to S.V.F., by the National Institute on Drug Abuse NIH (grant R61DA047023) to L.I.J., and by the University Cancer Research Fund, University of North Carolina at Chapel Hill to L.I.J.

■ ABBREVIATIONS

CBX, chromobox; DCM, dichloromethane; DMF, di-methyl formamide; DSF, differential scanning fluorimetry; H3, histone H3; H3K9me3, histone H3 lysine 9 trimethyl; H3K27me3, histone H3 lysine 27 trimethyl; HP1, heterochromatin Protein 1; Kme1, mono-methyl lysine; Kme2, di-methyl lysine; Kme3, tri-methyl lysine; MALDI, matrix-assisted laser desorption ionization; MeOH, methanol; OBOC, one-bead-one-compound; Pc, Polycomb; PTM, post-translational modification; SAR, structure–activity relationship; SPPS, solid-phase peptide synthesis; TBST, Tris-buffered saline + Tween-20; TOF, time of flight; UNC, University of North Carolina

■ REFERENCES

- (1) Arrowsmith, C. H.; Bountra, C.; Fish, P. V.; Lee, K.; Schapira, M. Epigenetic Protein Families: A New Frontier for Drug Discovery. *Nat. Rev. Drug Discovery* **2012**, *11*, 384–400.
- (2) Black, J. C.; Van Rechem, C.; Whetstone, J. R. Histone Lysine Methylation Dynamics: Establishment, Regulation, and Biological Impact. *Mol. Cell* **2012**, *48*, 491–507.

- (3) Mosammaparast, N.; Shi, Y. Reversal of Histone Methylation: Biochemical and Molecular Mechanisms of Histone Demethylases. *Annu. Rev. Biochem.* **2010**, *79*, 155–179.
- (4) Strahl, B. D.; Allis, C. D. The Language of Covalent Histone Modifications. *Nature* **2000**, *403*, 41–45.
- (5) Chi, P.; Allis, C. D.; Wang, G. G. Covalent Histone Modifications—Miswritten, Misinterpreted and Mis-Erased in Human Cancers. *Nat. Rev. Cancer* **2010**, *10*, 457–469.
- (6) Dawson, M. A.; Kouzarides, T. Cancer Epigenetics: From Mechanism to Therapy. *Cell* **2012**, *150*, 12–27.
- (7) Musselman, C. A.; Lalonde, M. E.; Côté, J.; Kutateladze, T. G. Perceiving the Epigenetic Landscape through Histone Readers. *Nat. Struct. Mol. Biol.* **2012**, *19*, 1218–1227.
- (8) Kamps, J. J.; Huang, J.; Poater, J.; Xu, C.; Pieters, B. J.; Dong, A.; Min, J.; Sherman, W.; Beuming, T.; Matthias Bickelhaupt, F.; Li, H.; Mecnović, J. Chemical Basis for the Recognition of Trimethyllysine by Epigenetic Reader Proteins. *Nat. Commun.* **2015**, *6*, 8911.
- (9) Kaustov, L.; Ouyang, H.; Amaya, M.; Lemak, A.; Nady, N.; Duan, S.; Wasney, G. A.; Li, Z.; Vedadi, M.; Schapira, M.; Min, J.; Arrowsmith, C. H. Recognition and Specificity Determinants of the Human Cbx Chromodomains. *J. Biol. Chem.* **2011**, *286*, 521–529.
- (10) Tchasovnikarova, I. A.; Timms, R. T.; Matheson, N. J.; Wals, K.; Antrobus, R.; Gottgens, B.; Dougan, G.; Dawson, M. A.; Lehner, P. J. GENE SILENCING. Epigenetic Silencing by the HUSH Complex Mediates Position-Effect Variegation in Human Cells. *Science* **2015**, *348*, 1481–1485.
- (11) Jacobs, S. A.; Taverna, S. D.; Zhang, Y.; Briggs, S. D.; Li, J.; Eissenberg, J. C.; Allis, C. D.; Khorasanizadeh, S. Specificity of the HP1 Chromo Domain for the Methylated N-Terminus of Histone H3. *EMBO J.* **2001**, *20*, 5232–5241.
- (12) Jacobs, S. A.; Khorasanizadeh, S. Structure of HP1 Chromodomain Bound to a Lysine 9-Methylated Histone H3 Tail. *Science* **2002**, *295*, 2080–2083.
- (13) Lachner, M.; O'Carroll, D.; Rea, S.; Mechtler, K.; Jenuwein, T. Methylation of Histone H3 Lysine 9 Creates a Binding Site for HP1 Proteins. *Nature* **2001**, *410*, 116–120.
- (14) Bannister, A. J.; Zegerman, P.; Partridge, J. F.; Miska, E. A.; Thomas, J. O.; Allshire, R. C.; Kouzarides, T. Selective Recognition of Methylated Lysine 9 on Histone H3 by the HP1 Chromo Domain. *Nature* **2001**, *410*, 120–124.
- (15) Nielsen, P. R.; Nietlispach, D.; Mott, H. R.; Callaghan, J.; Bannister, A.; Kouzarides, T.; Murzin, A. G.; Murzina, N. V.; Laue, E. D. Structure of the HP1 Chromodomain Bound to Histone H3 Methylated at Lysine 9. *Nature* **2002**, *416*, 103–107.
- (16) Fischle, W.; Wang, Y.; Jacobs, S. A.; Kim, Y.; Allis, C. D.; Khorasanizadeh, S. Molecular Basis for the Discrimination of Repressive Methyl-Lysine Marks in Histone H3 by Polycomb and HP1 Chromodomains. *Genes Dev.* **2003**, *17*, 1870–1881.
- (17) Munari, F.; Soeroes, S.; Zenn, H. M.; Schomburg, A.; Kost, N.; Schröder, S.; Klingberg, R.; Rezaei-Ghaleh, N.; Stützer, A.; Gelato, K. A.; Walla, P. J.; Becker, S.; Schwarzer, D.; Zimmermann, B.; Fischle, W.; Zweckstetter, M. Methylation of Lysine 9 in Histone H3 Directs Alternative Modes of Highly Dynamic Interaction of Heterochromatin Protein HHP1beta with the Nucleosome. *J. Biol. Chem.* **2012**, *287*, 33756–33765.
- (18) Suh, J. L.; Bsteh, D.; Si, Y.; Hart, B.; Weaver, T. M.; Pribitzer, C.; Lau, R.; Soni, S.; Ogana, H.; Rectenwald, J. M.; Norris, J. L.; Cholensky, S. H.; Sagum, C.; Umana, J. D.; Li, D.; Hardy, B.; Bedford, M. T.; Mumenthaler, S. M.; Lenz, H.-J.; Kim, Y.; Wang, G. G.; Pearce, K. H.; James, L. I.; Kireev, D. B.; Musselman, C. A.; Frye, S. V.; Bell, O. Reprogramming Cbx8-Prc1 Function With a Positive Allosteric Modulator. *bioRxiv* **2021**, DOI: 10.1101/2021.02.23.432388.
- (19) Wang, S.; Denton, K. E.; Hobbs, K. F.; Weaver, T.; McFarlane, J. M. B.; Connelly, K. E.; Gignac, M. C.; Milosevich, N.; Hof, F.; Paci, I.; Musselman, C. A.; Dykhuizen, E. C.; Krusemark, C. J. Optimization of Ligands Using Focused DNA-Encoded Libraries to Develop a Selective, Cell-Permeable CBX8 Chromodomain Inhibitor. *ACS Chem. Biol.* **2020**, *15*, 112–131.
- (20) Milosevich, N.; Gignac, M. C.; McFarlane, J.; Simhadri, C.; Horvath, S.; Daze, K. D.; Croft, C. S.; Dheri, A.; Quon, T. T. H.; Douglas, S. F.; Wulff, J. E.; Paci, I.; Hof, F. Selective Inhibition of CBX6: A Methyllysine Reader Protein in the Polycomb Family. *ACS Med. Chem. Lett.* **2016**, *7*, 139–144.
- (21) Simhadri, C.; Daze, K. D.; Douglas, S. F.; Quon, T. T. H.; Dev, A.; Gignac, M. C.; Peng, F.; Heller, M.; Boulanger, M. J.; Wulff, J. E.; Hof, F. Chromodomain Antagonists That Target the Polycomb-Group Methyllysine Reader Protein Chromobox Homolog 7 (CBX7). *J. Med. Chem.* **2014**, *57*, 2874–2883.
- (22) Denton, K. E.; Wang, S.; Gignac, M. C.; Milosevich, N.; Hof, F.; Dykhuizen, E. C.; Krusemark, C. J. Robustness of In Vitro Selection Assays of DNA-Encoded Peptidomimetic Ligands to CBX7 and CBX8. *SLAS Discovery* **2018**, *23*, 417–428.
- (23) Stuckey, J. I.; Dickson, B. M.; Cheng, N.; Liu, Y.; Norris, J. L.; Cholensky, S. H.; Tempel, W.; Qin, S.; Huber, K. G.; Sagum, C.; Black, K.; Li, F.; Huang, X. P.; Roth, B. L.; Baughman, B. M.; Senisterra, G.; Pattenden, S. G.; Vedadi, M.; Brown, P. J.; Bedford, M. T.; Min, J.; Arrowsmith, C. H.; James, L. I.; Frye, S. V. A Cellular Chemical Probe Targeting the Chromodomains of Polycomb Repressive Complex 1. *Nat. Chem. Biol.* **2016**, *12*, 180–187.
- (24) Stuckey, J. I.; Simpson, C.; Norris-Drouin, J. L.; Cholensky, S. H.; Lee, J.; Pasca, R.; Cheng, N.; Dickson, B. M.; Pearce, K. H.; Frye, S. V.; James, L. I. Structure-Activity Relationships and Kinetic Studies of Peptidic Antagonists of CBX Chromodomains. *J. Med. Chem.* **2016**, *59*, 8913–8923.
- (25) Lamb, K. N.; Bsteh, D.; Dishman, S. N.; Moussa, H. F.; Fan, H.; Stuckey, J. I.; Norris, J. L.; Cholensky, S. H.; Li, D.; Wang, J.; Sagum, C.; Stanton, B. Z.; Bedford, M. T.; Pearce, K. H.; Kenakin, T. P.; Kireev, D. B.; Wang, G. G.; James, L. I.; Bell, O.; Frye, S. V. Discovery and Characterization of a Cellular Potent Positive Allosteric Modulator of the Polycomb Repressive Complex 1 Chromodomain, CBX7. *Cell Chem. Biol.* **2019**, 1365.
- (26) Taverna, S. D.; Li, H.; Ruthenburg, A. J.; Allis, C. D.; Patel, D. J. How Chromatin-Binding Modules Interpret Histone Modifications: Lessons from Professional Pocket Pickers. *Nat. Struct. Mol. Biol.* **2007**, *14*, 1025–1040.
- (27) Weaver, T.; Morrison, E.; Musselman, C. Reading More than Histones: The Prevalence of Nucleic Acid Binding among Reader Domains. *Molecules* **2018**, *23*, 2614.
- (28) Yap, K. L.; Zhou, M. M. Structure and Mechanisms of Lysine Methylation Recognition by the Chromodomain in Gene Transcription. *Biochemistry* **2011**, *50*, 1966–1980.
- (29) Bosch-Presegue, L.; Raurell-Vila, H.; Thackray, J. K.; Gonzalez, J.; Casal, C.; Kane-Goldsmith, N.; Vizoso, M.; Brown, J. P.; Gomez, A.; Ausio, J.; Zimmermann, T.; Esteller, M.; Schotta, G.; Singh, P. B.; Serrano, L.; Vaquero, A. Mammalian HP1 Isoforms Have Specific Roles in Heterochromatin Structure and Organization. *Cell Rep.* **2017**, *21*, 2048–2057.
- (30) Eissenberg, J. C.; Elgin, S. C. The HP1 Protein Family: Getting a Grip on Chromatin. *Curr. Opin. Genet. Dev.* **2000**, *10*, 204–210.
- (31) Liu, Y.; Zhang, D. HP1a/KDM4A Is Involved in the Autoregulatory Loop of the Oncogene Gene c-Jun. *Epigenetics* **2015**, *10*, 453–459.
- (32) Liu, X.; Song, Z.; Huo, Y.; Zhang, J.; Zhu, T.; Wang, J.; Zhao, X.; Aikhionbare, F.; Zhang, J.; Duan, H.; Wu, J.; Dou, Z.; Shi, Y.; Yao, X. Chromatin Protein HP1 Interacts with the Mitotic Regulator Borealin Protein and Specifies the Centromere Localization of the Chromosomal Passenger Complex. *J. Biol. Chem.* **2014**, *289*, 20638–20649.
- (33) Maison, C.; Romeo, K.; Bailly, D.; Dubarry, M.; Quivy, J. P.; Almouzni, G. The SUMO Protease SENP7 Is a Critical Component to Ensure HP1 Enrichment at Pericentric Heterochromatin. *Nat. Struct. Mol. Biol.* **2012**, *19*, 458–460.
- (34) Mendez, D. L.; Kim, D.; Chruszcz, M.; Stephens, G. E.; Minor, W.; Khorasanizadeh, S.; Elgin, S. C. The HP1a Disordered C Terminus and Chromo Shadow Domain Cooperate to Select Target Peptide Partners. *ChemBioChem* **2011**, *12*, 1084–1096.

- (35) Mishima, Y.; Watanabe, M.; Kawakami, T.; Jayasinghe, C. D.; Otani, J.; Kikugawa, Y.; Shirakawa, M.; Kimura, H.; Nishimura, O.; Aimoto, S.; Tajima, S.; Suetake, I. Hinge and Chromoshadow of HP1 α Participate in Recognition of K9 Methylated Histone H3 in Nucleosomes. *J. Mol. Biol.* **2013**, *425*, 54–70.
- (36) Rosnoblet, C.; Vandamme, J.; Völkel, P.; Angrand, P. O. Analysis of the Human HP1 Interactome Reveals Novel Binding Partners. *Biochem. Biophys. Res. Commun.* **2011**, *413*, 206–211.
- (37) Azzaz, A. M.; Vitalini, M. W.; Thomas, A. S.; Price, J. P.; Blacketer, M. J.; Cryderman, D. E.; Zirbel, L. N.; Woodcock, C. L.; Elcock, A. H.; Wallrath, L. L.; Shogren-Knaak, M. A. Human Heterochromatin Protein 1 α Promotes Nucleosome Associations That Drive Chromatin Condensation. *J. Biol. Chem.* **2014**, *289*, 6850–6861.
- (38) Eissenberg, J. C.; Elgin, S. C. HP1 α : A Structural Chromosomal Protein Regulating Transcription. *Trends in Genetics*. Trends Genet March 2014, pp. 103–110. DOI: 10.1016/j.tig.2014.01.002.
- (39) Machida, S.; Takizawa, Y.; Ishimaru, M.; Sugita, Y.; Sekine, S.; Nakayama, J. I.; Wolf, M.; Kurumizaka, H. Structural Basis of Heterochromatin Formation by Human HP1. *Mol. Cell* **2018**, *69*, 385–397.e8. e8
- (40) Mendez, D. L.; Mandt, R. E.; Elgin, S. C. R. Heterochromatin Protein 1 α (HP1 α) Partner Specificity Is Determined by Critical Amino Acids in the Chromo Shadow Domain and C-Terminal Extension. *J. Biol. Chem.* **2013**, *288*, 22315–22323.
- (41) Liu, Y.; Qin, S.; Lei, M.; Tempel, W.; Zhang, Y.; Loppnau, P.; Li, Y.; Min, J. Peptide Recognition by Heterochromatin Protein 1 (HP1) Chromoshadow Domains Revisited: Plasticity in the Pseudosymmetric Histone Binding Site of Human HP1. *J. Biol. Chem.* **2017**, *292*, 5655–5664.
- (42) Ning, B.; Zhao, W.; Qian, C.; Liu, P.; Li, Q.; Li, W.; Wang, R. F. USP26 Functions as a Negative Regulator of Cellular Reprogramming by Stabilising PRC1 Complex Components. *Nat. Commun.* **2017**, *8*, 349.
- (43) Canzio, D.; Chang, E. Y.; Shankar, S.; Kuchenbecker, K. M.; Simon, M. D.; Madhani, H. D.; Narlikar, G. J.; Al-Sady, B. Chromodomain-Mediated Oligomerization of HP1 Suggests a Nucleosome-Bridging Mechanism for Heterochromatin Assembly. *Mol. Cell* **2011**, *41*, 67–81.
- (44) Hathaway, N. A.; Bell, O.; Hodges, C.; Miller, E. L.; Neel, D. S.; Crabtree, G. R. Dynamics and Memory of Heterochromatin in Living Cells. *Cell* **2012**, *149*, 1447–1460.
- (45) Fritsch, L.; Robin, P.; Mathieu, J. R. R.; Souidi, M.; Hinaux, H.; Rougeulle, C.; Harel-Bellan, A.; Ameyar-Zazoua, M.; Ait-Si-Ali, S. A Subset of the Histone H3 Lysine 9 Methyltransferases Suv39h1, G9a, GLP, and SETDB1 Participate in a Multimeric Complex. *Mol. Cell* **2010**, *37*, 46–56.
- (46) Lin, C.-H.; Paulson, A.; Abmayr, S. M.; Workman, J. L. HP1 α Targets the Drosophila KDM4A Demethylase to a Subset of Heterochromatic Genes to Regulate H3K36me3 Levels. *PLoS One* **2012**, *7*, No. e39758.
- (47) Maison, C.; Almouzni, G. HP1 and the Dynamics of Heterochromatin Maintenance. *Nat. Rev. Mol. Cell Biol.* **2004**, *5*, 296–305.
- (48) Chu, L.; Huo, Y.; Liu, X.; Yao, P.; Thomas, K.; Jiang, H.; Zhu, T.; Zhang, G.; Chaudhry, M.; Adams, G.; Thompson, W.; Dou, Z.; Jin, C.; He, P.; Yao, X. The Spatiotemporal Dynamics of Chromatin Protein HP1 α Is Essential for Accurate Chromosome Segregation during Cell Division. *J. Biol. Chem.* **2014**, *289*, 26249–26262.
- (49) Ruppert, J. G.; Samejima, K.; Platani, M.; Molina, O.; Kimura, H.; Jeyaprakash, A. A.; Ohta, S.; Earnshaw, W. C. HP1 α Targets the Chromosomal Passenger Complex for Activation at Heterochromatin before Mitotic Entry. *EMBO J.* **2018**, *37* (), DOI: 10.15252/embj.201797677.
- (50) Romeo, K.; Louault, Y.; Cantaloube, S.; Loiodice, I.; Almouzni, G.; Quivy, J. P. The SENP7 SUMO-Protease Presents a Module of Two HP1 Interaction Motifs That Locks HP1 Protein at Pericentric Heterochromatin. *Cell Rep.* **2015**, *10*, 771–782.
- (51) Lai, X.; Deng, Z.; Guo, H.; Zhu, X.; Tu, W. HP1 α Is Highly Expressed in Glioma Cells and Facilitates Cell Proliferation and Survival. *Biochem. Biophys. Res. Commun.* **2017**, *490*, 415–422.
- (52) Vad-Nielsen, J.; Nielsen, A. L. Beyond the Histone Tale: HP1 α Deregulation in Breast Cancer Epigenetics. *Cancer Biol. Ther.* **2015**, *16*, 189–200.
- (53) Frye, S. V. The Art of the Chemical Probe. *Nat. Chem. Biol.* **2010**, *6*, 159–161.
- (54) Arrowsmith, C. H.; Audia, J. E.; Austin, C.; Baell, J.; Bennett, J.; Blagg, J.; Bountra, C.; Brennan, P. E.; Brown, P. J.; Bunnage, M. E.; Buser-Doepner, C.; Campbell, R. M.; Carter, A. J.; Cohen, P.; Copeland, R. A.; Cravatt, B.; Dahlin, J. L.; Dhanak, D.; Edwards, A. M.; Frederiksen, M.; Frye, S. V.; Gray, N.; Grimshaw, C. E.; Hepworth, D.; Howe, T.; Huber, K. V.; Jin, J.; Knapp, S.; Kotz, J. D.; Kruger, R. G.; Lowe, D.; Mader, M. M.; Marsden, B.; Mueller-Fahrnow, A.; Muller, S.; O'Hagan, R. C.; Overington, J. P.; Owen, D. R.; Rosenberg, S. H.; Roth, B.; Ross, R.; Schapira, M.; Schreiber, S. L.; Shoichet, B.; Sundstrom, M.; Superti-Furga, G.; Taunton, J.; Toledo-Sherman, L.; Walpole, C.; Walters, M. A.; Willson, T. M.; Workman, P.; Young, R. N.; Zuercher, W. J. The Promise and Peril of Chemical Probes. *Nat. Chem. Biol.* **2015**, *11*, 536–541.
- (55) Workman, P.; Collins, I. Probing the Probes: Fitness Factors for Small Molecule Tools. *Chem. Biol.* **2010**, *17*, 561–577.
- (56) Barnash, K. D.; Lamb, K. N.; Stuckey, J. I.; Norris, J. L.; Cholensky, S. H.; Kireev, D. B.; Frye, S. V.; James, L. I. Chromodomain Ligand Optimization via Target-Class Directed Combinatorial Repurposing. *ACS Chem. Biol.* **2016**, *11*, 2475–2483.
- (57) Kwon, Y. U.; Kodadek, T. Quantitative Evaluation of the Relative Cell Permeability of Peptoids and Peptides. *J. Am. Chem. Soc.* **2007**, *129*, 1508–1509.
- (58) Tan, N. C.; Yu, P.; Kwon, Y. U.; Kodadek, T. High-Throughput Evaluation of Relative Cell Permeability between Peptoids and Peptides. *Bioorg. Med. Chem.* **2008**, *16*, 5853–5861.
- (59) Barnash, K. D.; The, J.; Norris-Drouin, J. L.; Cholensky, S. H.; Worley, B. M.; Li, F.; Stuckey, J. I.; Brown, P. J.; Vedadi, M.; Arrowsmith, C. H.; Frye, S. V.; James, L. I. Discovery of Peptidomimetic Ligands of EED as Allosteric Inhibitors of PRC2. *ACS Comb. Sci.* **2017**, *19*, 161–172.
- (60) Barnash, K. D. A Combinatorial Platform for The Optimization of Peptidomimetic Methyl-Lysine Reader Antagonists, University of North Carolina at Chapel Hill. DOI: 10.17615/7swt-cw22.
- (61) Niesen, F. H.; Berglund, H.; Vedadi, M. The Use of Differential Scanning Fluorimetry to Detect Ligand Interactions That Promote Protein Stability. *Nat. Protoc.* **2007**, *2*, 2212–2221.
- (62) Rectenwald, J. M.; Hardy, P. B.; Norris-Drouin, J. L.; Cholensky, S. H.; James, L. I.; Frye, S. V.; Pearce, K. H. A General TR-FRET Assay Platform for High-Throughput Screening and Characterizing Inhibitors of Methyl-Lysine Reader Proteins. *SLAS Discovery* **2019**, *24*, 693–700.
- (63) King, H. W.; Fursova, N. A.; Blackledge, N. P.; Klose, R. J. Polycomb Repressive Complex 1 Shapes the Nucleosome Landscape but Not Accessibility at Target Genes. *Genome Res.* **2018**, *28*, 1494–1507.
- (64) Simon, J. A.; Kingston, R. E. Occupying Chromatin: Polycomb Mechanisms for Getting to Genomic Targets, Stopping Transcriptional Traffic, and Staying Put. *Mol. Cell* **2013**, *49*, 808–824.
- (65) Astle, J. M.; Simpson, L. S.; Huang, Y.; Reddy, M. M.; Wilson, R.; Connell, S.; Wilson, J.; Kodadek, T. Seamless Bead to Microarray Screening: Rapid Identification of the Highest Affinity Protein Ligands from Large Combinatorial Libraries. *Chem. Biol.* **2010**, *17*, 38–45.
- (66) Gao, Y.; Kodadek, T. Synthesis and Screening of Stereochemically Diverse Combinatorial Libraries of Peptide Tertiary Amides. *Chem. Biol.* **2013**, *20*, 360–369.